Università Cattolica del Sacro Cuore
Sede di Brescia

Facoltà di Scienze Matematiche, Fisiche e Naturali
Corso di Laurea di Primo Livello in Fisica

Second Harmonic Generation in KNS ceramic powder

Relatore:
Dott. Gabriele Ferrini
Correlatore:
Dott. Claudio Giannetti

Laureando: **Davide Bossini**
mat. 3302565

Anno Accademico 2006/2007

Contents

1. Introduction

In many applications coherent light is required at wavelength not available with laser systems, that's why optical converters are widespread devices. Standard converters have an extremely high efficiency (close to 100%) but they are very expensive and they need careful alignment of the optical set-up to work successfully.

In recent years many works have demonstrated that polycrystalline materials exhibit second harmonic converters behavior, even if the conversion efficiency is much lower than in the case of the standard non-linear crystals.

Some ceramic glasses has shown optical converters features ([3, 2]), for example the potassium niobium silicate ceramic glasses (KNS), studied in [1]. They are polycrystalline transparent materials that consist in a glassy matrix, where nano-crystalline elements are disposed randomly.

The size and the number of the domains determine the overall second harmonic generation efficiency of the ceramic glass.

The glasses can be grounded to powder in order to establish the value of the domain size which involves the maximum conversion efficiency ([2, 5]).

This size is the coherence length of the material. Hence the glasses can be produced with coherence length sized domains.

Our first aim was to analyze the optical properties of four ceramic glasses (NaNS, LiKNS, KNaNS and KNS) , in order to compare their second harmonic generation (SHG) efficiency with the samples analyzed in [1].

However the main goal of this work is determine the coherence length of KNS. We had four powder samples with different grain size; we wanted to find the second harmonic intensity trend in function of the grain size.

2. Characterization of samples

In this work we analyzed samples produced by the staff of the Department of Materials and Production Engineering at the University of Naples.

2.1 Non-linearity of polycrystalline materials

The non-linear behavior of amorphous or nano-crystalized ceramic materials is the subject of some works in recent years ([2, 5, 4, 3]).

The potassium niobium silicate (KNS) glasses are polycrystalline materials in which second harmonic generation process has been observed ([8]). KNS glasses were studied both amorphous and nanostructured. The amorphous nature was revealed by x-ray diffraction analysis; the nanostructured glasses were obtained with an appropriate heat treatment near T_g (glass solidification temperature). The nanostructuring of KNS is in the scale of $5 - 20nm$ and it was revealed by small-angle neutron scattering. In contrast to initial KNS glasses, which were *as-quenched* (non subjected to heat treatment), nanostructured glasses exhibit Second Harmonic Generation (SHG)

activity, as it is reported in [8]. The following step was the study of SHG in glasses subjected to different heat treatments, in which both the temperature and the duration of the annealing process changed. This is the topic of [1]. The SHG seems to be due to the nanocrystals that compose the material, the efficiency of the process is related to the size of the nanocrystallities. The authors of [2] concluded that the SHG in this material originates from the abrupt changes in optical susceptibility at the interface between the glass and crystal, together with the higher-order nonlinear response.

Nowadays there isn't a physical model that allows the interpretation of SHG in KNS glasses, even if a first attempt was done ([8]). The main obstacle consists in writing the polarization vector for this kind of materials, because the form of their dielectric tensor isn't known.

The powders obtained from ceramic materials were analyzed in some works ([2, 5]). It was observed that the efficiency of the second harmonic generation process depends on the grain size.

2.2 Production of samples

We used two kind of samples: ceramic glasses and ceramic powder.

We analyzed four ceramic glasses:

- NaNS as-quenched;
- LiKNS as-quenched;
- KNaNS as-quenched;
- KNS 23-27-50 subject to annealing process of 2h at 680°C.

The KNS sample was previously studied in [1], it resulted to be the most performing sample among all the KNS ceramic glasses analyzed in that work.

The three as-quenched samples are composed by nanocrystals precipitate on a glassy matrix, with the melt-quench technique well described in [10, 9]. These glasses are pale yellow transparent.

With the same technique four KNS ceramic glasses (23-27-50) were produced by the staff of the Department of Materials and Production Engineering at the University of Naples. The resulting glass samples were ground into powder with an agate mortar and pestled and sieved into four distinct grain size (d) ranges:

- $d < 32\mu m$;
- $32 < d < 45\mu m$;
- $45 < d < 90\mu m$;
- $90 < d < 125\mu m$;

2.3 Theoretical introduction

In this section we give only some basic concepts about the second harmonic generation process in non conducting media, we don't use the quantum theory of nonlinear optics.

2.3.1 Mechanical approach to second harmonic generation

A mechanical model suitable to describe the interaction between light and matter is the Lorentz oscillator; it is a classical model, but it can forecast results that are compatible with experimental data.

The main idea of this approach is considering the electrons in a dielectric isotropic medium like a damped oscillator, driven by an external drive force.

We now seek the behavior of an electron subject to a confinement potential, containing higher-order non-quadratic terms. We shall suppose that the confinement potential $U(x)$ is one dimensional, so

$$U(x) = \frac{1}{2}m\omega_0^2 x^2 + \frac{1}{3}mDx^3 \tag{2.1}$$

where ω_0 is the natural oscillation frequency of the oscillator in the linear regime, m is the electron mass and D is the non-linear coefficient. The system is subjected to a dipolar electric driving force:

$$F = qE\cos\omega t = \frac{qE}{2m}(e^{i\omega t} + c.c.) \tag{2.2}$$

where *c.c.* designates the complex conjugate.

The motion of the particle $x(t)$ is described by the differential equation:

$$\ddot{x} + \gamma\dot{x} + \omega_0^2 x + Dx^2 = \frac{qE}{2m}(e^{i\omega t} + c.c.) \tag{2.3}$$

where γ is the friction coefficient. As the motion of the particle must be periodic (with frequency ω and relative harmonics) we can make an harmonic analysis of $x(t)$ by writing it as:

$$x(t) = \frac{1}{2}(x_0 + x_1 e^{i\omega t} + x_2 e^{i2\omega t} + ... + c.c.) \tag{2.4}$$

We will assume that $x_0 = 0$. Substituting 2.4 in 2.3 we obtain:

$$\begin{aligned} &-\frac{\omega^2}{2}(x_1 e^{i\omega t}+c.c.)-2\omega^2(x_2 e^{i2\omega t}+c.c.)+\frac{i\omega\gamma}{2}(x_1 e^{i\omega t}+c.c.)+i\omega\gamma(x_2 e^{i2\omega t}+c.c.) \\ &+ \frac{\omega_0^2}{2}(x_1 e^{i\omega t} + c.c.) + \frac{\omega_0^2}{2}(x_2 e^{i2\omega t} + c.c.) + \frac{D}{4}(x_1^2 e^{2i\omega t} + 2x_1 x_2^* e^{-i\omega t} \\ &+ x_1 x_1^* + x_2 x_2^* + 2x_1 x_2 e^{3i\omega t} + x_2^2 e^{4i\omega t} + c.c.) = \frac{qE}{2m}(e^{i\omega t} + c.c.) \end{aligned} \tag{2.5}$$

We will first consider the linear response, so the terms in $e^{i\omega t}$ and neglect those in D. Hence we find:

$$x_1 = \frac{qE}{m}\frac{1}{(\omega_0^2 - \omega^2) + i\omega\gamma} \approx \frac{qE}{2\omega m}\frac{1}{(\omega_0 - \omega) + i\gamma/2} \tag{2.6}$$

for $\omega \approx \omega_0$. The motion $x_1(t) = \frac{1}{2}x_1 e^{i\omega t} + c.c.$ gives rise to a linear polarization in the medium:

$$P_1(t) = Nqx_1(t) = \frac{Nq}{2}(x_1 e^{i\omega t} + c.c.) \tag{2.7}$$

where N is the volumetric density of the systems which interact with the wave.

It is useful remind the relation between polarization and susceptibility:

$$P = \epsilon_0 \chi E(t) \approx \frac{\epsilon_0}{2}(\chi^{(\omega)} E e^{i\omega t} + \chi^{(2\omega)} E^2 e^{i2\omega t} + c.c.) \tag{2.8}$$

where the RHS is the expansion of the vector P around $E = 0$. Thus we can express the polarization in the medium as follows:

$$P_1(t) = \frac{\epsilon_0}{2}(\chi_1^{(\omega)} E e^{i\omega t} + c.c.) \tag{2.9}$$

which leads to:

$$\chi_1^{(\omega)} = \frac{Nq^2}{2\omega m \epsilon_0} \frac{1}{(\omega_0 - \omega) + i\gamma/2} \tag{2.10}$$

From (2.8), we define the non-linear second-order susceptibility as:

$$P_2(t) = \frac{\epsilon_0}{2}(\chi_2^{(2\omega)} E^2 e^{i2\omega t} + c.c.) = \frac{Nq}{2}(x_2 e^{i2\omega t} + c.c.) \tag{2.11}$$

The term in x_2 is generated by the non-linear quadratic term Dx^2 in (2.3). An expression for it can be obtained through (2.5) by identifying terms in $e^{2i\omega t}$:

$$x_2(-4\omega^2 + 2i\omega\gamma + \omega_0^2) = -\frac{1}{2} D x_1^2 \tag{2.12}$$

In this last equation it's clear that the term in x_1^2 drives the 2ω motion of the electron. Employing (2.6) in (2.12), we get:

$$\begin{aligned} x_2 &= -\frac{q^2 D}{2m^2} \frac{1}{[(\omega_0^2 - \omega^2) + i\omega\gamma]^2[(\omega_0^2 - 4\omega^2) + 2i\omega\gamma]} E^2 \\ &\approx -\frac{q^2 D}{24 m^2 \omega^3} \frac{1}{[(\omega_0 - \omega) + i\gamma/2]^2[(\omega_0 - 2\omega) + (2/3)i\gamma]} E^2 \end{aligned} \tag{2.13}$$

After substituting this last equation in (2.11) we can write the second-order non-linear susceptibility:

$$\chi_2^{(2\omega)} = -\frac{Nq^3D}{24\epsilon_0 m^2\omega^3}\,\frac{1}{[(\omega_0-\omega)+i\gamma/2]^2[(\omega_0-2\omega)+(2/3)i\gamma]} \tag{2.14}$$

There is an observation on (2.14) that is worthy of mention: the system is doubly resonant, there is a resonance at $\omega = \omega_0$ and at $\omega = 2\omega_0$. Besides when comparing (2.10) and (2.14), we can see that this model predicts the following relationship between linear and non-linear optical susceptibilities:

$$\frac{\chi_2^{(2\omega)}}{(\chi_1^{(\omega)})^2\chi_1^{(2\omega)}\epsilon_0^2} = \frac{mD}{2N^2q^3} = \delta^{(2\omega)} \tag{2.15}$$

The parameter $\delta^{(2\omega)}$ is known as the *Miller parameter* and it should be very similar for all materials, and actually it is. In fact $\delta^{(2\omega)} \approx 3 - 8\times10^9$SI.

Finally, we have to underline that the quantity χ_2 is a tensor. If the fundamental wave has components (E_x, E_y, E_z), the second harmonic wave will have components (P_x, P_y, P_z) which in the most general case, will be determined by all quadratic combinations between the components E_x, E_y, and E_z, so:

$$\begin{bmatrix} P_x \\ P_y \\ P_Z \end{bmatrix} = \epsilon_0\chi_2^{(2\omega)} \begin{bmatrix} E_x^2 \\ E_y^2 \\ E_z^2 \\ E_yE_z \\ E_zE_x \\ E_xE_y \end{bmatrix} \tag{2.16}$$

The properties of the tensor $\chi_2^{(2\omega)}$ depend strongly on the symmetries of a given crystal.

2.3.2 **Electromagnetic approach to non-linear optical interaction**

The anharmonic displacement of electrons in a non-linear material subject to excitation by an electromagnetic wave leads to light emission at frequency 2ω, 3ω, and following harmonics. The calculation of the optical emission due to these non-linear source terms is taken into account using the Maxwell's equation. In the absence of free charges ($\rho = 0$) and conducting currents ($j = 0$), the Maxwell's equations are:

$$\begin{aligned} &\nabla \cdot E = 0, && \nabla \cdot B = 0 \\ &\nabla \times E = -\frac{\partial}{\partial t} B, && \nabla \times B = \mu_0 \frac{\partial}{\partial t} D = \mu_0 \frac{\partial}{\partial t}(\epsilon_0 E + P) \end{aligned} \tag{2.17}$$

where P is the polarization vector and is the sum of the linear polarization P_l given by (2.9) or $P_l = \epsilon_0 E(n_{op}^2 - 1)$, with $n_{op}^2 = 1 + \chi_L$, and the non-linear polarization P_{nl} as given in (2.11). We also make the assumption that the media we consider aren't magnetic. From equations (2.17) we can derive the propagation equation, that is:

$$\nabla^2 E - \left(\frac{n_{op}}{c}\right) \frac{\partial^2}{\partial t^2} E = \mu_0 \frac{\partial^2}{\partial t^2} P_{nl} \tag{2.18}$$

We will consider three electromagnetic waves with frequencies ω_1, ω_2, ω_3, which propagate within a non-linear crystal. We shall suppose that the system is one dimensional and the propagation occur only along the z-axis.

We can write these three waves as *envelope* functions in the following way:

$$E^{(\omega)}(z,t) = \frac{1}{2}[E_i(z)e^{i(\omega_i t - k_i z)} + c.c.] \qquad i = 1,\, 2,\, 3. \tag{2.19}$$

We have to put in evidence that the envelope function approximation (SVEA) establishes that the amplitude variations $E_i(z)$ are small in comparison to the scale of the involved wavelengths $\lambda_i = 2\pi/k_i$. This means that:

$$\left|\frac{dE_i}{dz}k_i\right| \gg \frac{d^2E_i}{dz^2} \tag{2.20}$$

We recall the dispersion relation

$$\omega_i = k_i\frac{c}{n_i} \tag{2.21}$$

that can be derived from the solution of the Maxwell's linear equations (without the source term we have in (2.18)).

The three waves interact in the crystal through the effect of non-linear polarization: we shall suppose that the non-linear polarization vector is oriented along the y-axis and we will only consider its norm P_{nl}.

Among all the possible frequency mixings, we are interested only in the sum frequency process, because second harmonic generation is a particular case of this phenomenon. The non-linear source term has terms in $E^{\omega_1}(z,t)E^{\omega_2}(z,t)$ which will generate terms of angular frequency
$\omega_3 = \omega_1 + \omega_2$.

The non-linear source term corresponding to the sum frequency mechanism is obtained from (2.11):

$$P_{nl}(z,t) = \frac{\epsilon_0 \chi_2}{2}[E_1(z)E_2(z)e^{i(\omega_1+\omega_2)t-(k_3-k_2)z} + c.c.] \tag{2.22}$$

Even if in this notation we write χ_2, it must be underlined that the susceptibility is different for every frequency mixing process, i.e. $\chi_2^{2\omega} \neq \chi_2^{\omega_3-\omega_2}$.

We have to substitute (2.22) as the source term in the propagation equation (2.18). We shall calculate separately the first term of this equation:

$$\begin{aligned}\frac{\partial^2}{\partial z^2}E^{\omega_3}(z,t) &= \frac{1}{2}\{\frac{d^2}{dz^2}[E_3(z)e^{i(\omega_3 t-k_3 z)}] + c.c\} \\ &= \frac{1}{2}\left[\left(\frac{d^2}{dz^2}E_3 - 2ik_3\frac{d}{dz}E_3 - k_3^2E_3\right)e^{i(\omega_3 t-k_3 z)} + c.c.\right] \\ &\approx \frac{1}{2}\left[\left(-2ik_3\frac{d}{dz}E_3 - k_3^2E_3\right)e^{i(\omega_3 t-k_3 z)} + c.c.\right]\end{aligned} \tag{2.23}$$

where we used the approximation (2.20). The propagation equation , (2.18), may therefore be written as:

$$\begin{aligned}&-\frac{1}{2}\left(2ik_3\frac{d}{dz}E_3 + k_3^2E_3\right)e^{i(\omega_3 t-k_3 z)} + c.c. \\ &= -\left(\frac{\omega_3 n_3}{c}\right)\left(\frac{E_3}{2}e^{i(\omega_3 t-k_3 z)} + c.c.\right) - \frac{\epsilon_0\mu_0\omega_3^2}{2}(\chi_2 E_1 E_2 e^{i(\omega_3 t+(k_1-k_2)z)})\end{aligned} \tag{2.24}$$

As $\omega_3 = k_3 c/n_3$ this equation can be simplified, we can rewrite it considering only the spatial dependence:

$$ik_3\frac{d}{dz}E_3 e^{-ik_3 z} + c.c. = \frac{\mu_0\epsilon_0\omega_3^2}{2}[\chi_2 E_1 E_2 e^{-i(k_1-k_2)z} + c.c.] \tag{2.25}$$

Thus we can describe the variation of the complex amplitude $E_3(z)$ in the material, as a function of the amplitude of the two source-waves $E_1(z)$ and $E_2(z)$. In the sum frequency process the amplitudes $E_1(z)$, $E_2(z)$, and $E_3(z)$ are related by the following differential equation:

$$\frac{d}{dz}E_3 = -i\frac{\omega_3}{2n_3c}\chi_2 E_1 E_2 e^{i\Delta kz} \tag{2.26}$$

where $\Delta k = k_3 - k_1 - k_2$, it is called *phase mismatch*.

2.3.3 **Electromagnetic approach to second harmonic generation**

In this section we describe the particular case where $\omega = \omega_1 = \omega_2$ and $\omega_3 = 2\omega$. This situation corresponds to the optical second harmonic generation. Equation (2.26) becomes:

$$\begin{aligned}
\frac{d}{dz}E_\omega &= -i\,\frac{\omega}{2n_\omega c}\,\chi_2 E_{2\omega} E_\omega^* e^{-i\Delta kz} \\
\frac{d}{dz}E_{2\omega} &= -i\,\frac{\omega}{n_{2\omega}c}\,\chi_2 E_\omega^2 e^{i\Delta kz}
\end{aligned} \tag{2.27}$$

The first equation of (2.27) comes from the generalized equation for the difference frequency generation, whose derivation can be found in [6].

The origin of the Δk term is that the source field $P_{2\omega}$ is synchronous with the field E_ω (which generates it): the propagation speed of the E_ω field is c/n_ω, while the field $E_{2\omega}$ propagates with speed $c/n_{2\omega}$.

We suppose that the non-linear conversion efficiency is weak enough to reasonably consider $E_\omega(z)$ constant over the interaction volume; so $E_\omega(z) = E_0$. The second equation of (2.27) can be easily integrated along the interaction path (the non-linear crystal length from 0 to L) to find:

$$E_{2\omega}(L) = -i\frac{\omega}{n_{2\omega}c}\,\chi_2 E_0^2\,\frac{e^{i\Delta kL}-1}{i\Delta k} = -i\frac{\omega}{n_{2\omega}c}\,\chi_2 E_0^2\,e^{\frac{i\Delta kL}{2}}\;\frac{e^{\frac{i\Delta kL}{2}}-e^{\frac{-i\Delta kL}{2}}}{i\Delta k} \tag{2.28}$$

multiplying and dividing by $L/2$ we get

$$\begin{aligned} E_{2\omega}(L) &= -i\frac{\omega}{n_{2\omega}c}\,\chi_2 E_0^2\,e^{\frac{i\Delta kL}{2}}\,\frac{L}{2}\;\frac{e^{\frac{i\Delta kL}{2}}-e^{\frac{-i\Delta kL}{2}}}{\frac{i\Delta kL}{2}} = -i\frac{\omega}{n_{2\omega}c}\,\chi_2 E_0^2\,e^{\frac{i\Delta kL}{2}}L\;\frac{\sin\left(\frac{\Delta kL}{2}\right)}{\frac{\Delta kL}{2}} \\ &= -i\frac{\omega}{n_{2\omega}c}\,\chi_2 E_0^2\,e^{\frac{i\Delta kL}{2}}L\;\sinh\left(\frac{\Delta kL}{2}\right) \end{aligned} \tag{2.29}$$

We are more interested in the optical power converted into second harmonic radiation, which relates to the amplitude $E_{2\omega}$ according to:

$$I_{2\omega} = \frac{1}{2Z_0}n_{2\omega}|E_{2\omega}(L)|^2 \tag{2.30}$$

where Z_0 is the vacuum impedance ($Z_0 = (\mu_0/\epsilon_0)^{1/2} = 377\Omega$). The second harmonic frequency conversion efficiency is then:

$$\frac{I_{2\omega}}{I_\omega} = \frac{2Z_0 I_\omega}{n_\omega^2 n_{2\omega}}\left[\frac{\omega}{c}\chi_2 L\right]^2 \sinh\left(\frac{\Delta kL}{2}\right)^2 = \frac{8\pi^2 Z_0 I_\omega}{n_\omega^2 n_{2\omega}}\left[\frac{L}{\lambda}\chi_2\right]^2 \sinh\left(\frac{\Delta kL}{2}\right)^2 \tag{2.31}$$

This last equation shows clearly the main role played by the phase mismatch Δk. If this term is null, the conversion efficiency is proportional

quadratically to the interaction length L (because $\sinh(0) = 1$), and there is a permanent exchange of energy between the fundamental wave and the second harmonic wave along the interaction length. If Δk isn't zero, the efficiency depends on $\sinh(\Delta kL/2)$, which oscillates periodically along the interaction path. In this situation, the energy periodically cycles between both waves during propagation in the crystal. The distance L_c at the end of which the energy transfer is at a maximum value is given by $\Delta kL_c = \pi$, so:

$$L_c = \frac{\lambda_0}{4(n_{2\omega} - n_\omega)} \tag{2.32}$$

where λ_0 is the vacuum wavelength of the fundamental radiation. The quantity L_c is called *coherence length*. Thus the best way to perform high conversion efficiency second harmonic generation process consists in the phase-matching condition.

2.3.4 **Phase-matching**

The phase-matching condition may be seen in atomic scale as the constructive interference of the second harmonic waves generated by different atoms (figure 2.1a).

The condition of phase matching ($k_{2\omega} - 2k_\omega = 0$) requires that the two waves, the fundamental and the second harmonic, should travel with the same velocity. But this doesn't occur because of the normal dispersion, in fact the speed of a wave is

$$v = \frac{\omega}{k} = \frac{c}{n} \tag{2.33}$$

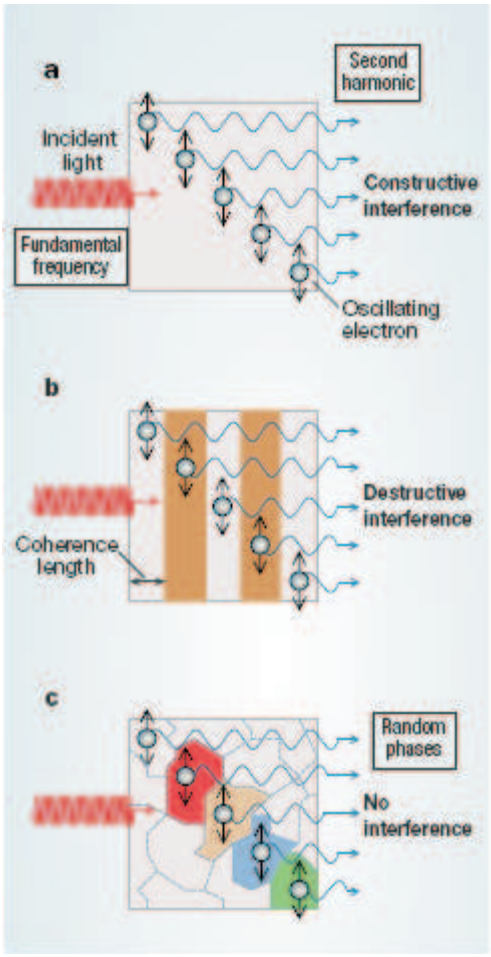

Figure 2.1: Second harmonic generation in different materials

The most common approach is to make use of birefringent crystal: in such a crystal the polarization of the light end its direction of propagation influence the speed of the wave. Hence for some special choice of polarization and direction, phase-matching can be achieved. A complete treatment on the phase-matching obtained with birefringence can be found in [6].

This approach can't be applied in isotropic crystals, because they lack of optical birefringence: in successive layers defined by the coherence length the second harmonic waves generated have opposite phases, which means

destructive interference (figure 2.1b). In a sample with an even number of coherence-length layers, the second harmonic signal vanishes; for an odd number of layers it is only as strong as if the total length of the sample were equal to the coherence length, because only the last layer contributes to the total signal.

The solution can be represented by microstructured samples made up of layers of coherence length width with alternating crystal orientation. The result is that the alternating sign of the non-linear interaction makes the interference of waves generated by successive layers globally constructive. This situation is called *quasi-phase-matching*. However the technology required to produce such a material is undeveloped and expensive.

The possibility that random structures might be appropriate had already been noted ([12, 13]). Recently it has been considered ([5]) the random quasi-phase-matching in polycrystalline disordered materials. The samples analyzed in [5] contain a large number of single-crystal domain with random orientations, random shapes and random sizes. The frequency-converted waves generated by different domain achieve random phases and interfere neither constructively nor destructively. The total intensity of the generated wave is then the sum of the intensities arising from individual domains; it grows linearly with the number of domains or the length of the sample (figures (2.1c) and (2.2)).

Quasi-phase-matching is worth to be treated a bit more deeply. The idea behind this approach is to modulate spatially the optical non-linearity with some period (Γ) to supply a quasi-wavevector $K = 2\pi/\Gamma$.

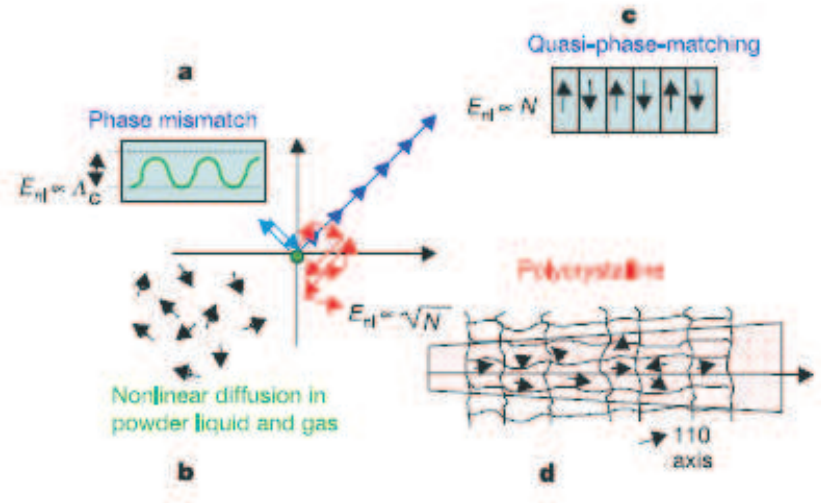

Figure 2.2: Different phase-matching situation: (**a**) The transfer of energy between the waves oscillates with a period of $2L_c$ leading to a small conversion efficiency. (**b**) In a totally disordered material (powder, gas, liquid) each particles behave independently, scattering the non-linearly generated fields in an incoherent way. (**c**) In quasi-phase-matched materials the orientation of the crystal is rotated every L_c. The energy transfer E_{nl} adds up constructively with the propagating distance ($E_{nl} \propto N$, where N is the number of grains). (**d**) In polycrystalline materials there is a coherent growth of the non-linear generated fields according to $E_{nl} \propto \sqrt{N}$.

Thus the quasi-phase-matching condition consists in providing a quasi-wavevector such that $k_{2\omega} - 2k_{\omega} = K$.

The spatial modulation for $\chi_2(z)$ can be written as:

$$\chi_2(z) = \chi_2 f(z) \tag{2.34}$$

where $f(z)$ is aperiodic function which oscillates between -1 and $+1$.

We have to introduce this change of the susceptibility in (2.27), that is the equation that rules the evolution of the second harmonic field $E_{2\omega}$; so we obtain:

$$\frac{d}{dz}E_{\omega} = -i\,\frac{\omega\chi_2}{n_{2\omega}c}\,E_{\omega}^2 f(z)e^{i\Delta kz} \tag{2.35}$$

The converted field strength $E_{2\omega}$ at the end of a propagation distance L is then:

$$E_{2\omega}(L) = -i\,\frac{\omega\chi_2}{n_{2\omega}c}\,E_{\omega}^2 \int_0^L f(z)e^{i\Delta kz}dz \tag{2.36}$$

Expanding $f(z)$ as a Fourier series with period Γ:

$$f(z) = \sum_n f_n e^{-in(2\pi/\Gamma)z} \tag{2.37}$$

Equation (2.38) then gives:

$$E_{2\omega}(L) = -i\,\frac{\omega\chi_2}{n_{2\omega}c}\,E_{\omega}^2 \sum_n f_n \int_0^L e^{i(\Delta kz - 2n\pi/\Gamma)}dz \tag{2.38}$$

in this last equation is clear the role played by the periodic modulation of susceptibility. If an integer n exists such that:

$$k_{2\omega} - k_{\omega} = \frac{2n\pi}{\Gamma} \tag{2.39}$$

from (2.38) it follows that:

$$E_{2\omega}(L) = -i\,\frac{\omega(f_n\chi_2)L}{n_{2\omega}c}\,E_{\omega}^2 \tag{2.40}$$

Comparing (2.39) with the expression for the coherence length (2.32), we see that the modulation periods are multiples of L_c:

$$\Gamma = 2nL_c \tag{2.41}$$

Expression (2.40) shows that the medium behaves like it is phase-matched, but with an effective non-linear susceptibility given by:

$$\chi_2^{eff} = |f_n|\chi_2 \tag{2.42}$$

where f_n is the Fourier series term for the periodic function $f(z)$ given by:

$$f_n = \frac{1}{\Gamma}\int_0^{\Gamma} f(z)e^{in(2\pi/\Gamma)z}dz \tag{2.43}$$

If $f(z)$ is a sinusoidal function ($f(z) = \sin(2\pi z/\Gamma)$), then $f_n = f_1 = 1/2$ and $\chi_2^{eff} = \chi_2/2$.

Looking at figure (2.2), it is clear that a more realistic approach involves modulating the non-linear susceptibility by periodically reversing the direction of the non-linearity so that $f(z) = +1$ between 0 and $\Gamma/2$, and $f(z) = +1$ between $\Gamma/2$ and Γ.

Integration of (2.43) leads to:

$$\chi_2^{eff} = \frac{2}{\pi}\chi_2 \tag{2.44}$$

The direction of the non-linearity is inverted before the cyclic energy transfer begins from the second harmonic wave to the fundamental wave.

3. Experimental set-up

We have performed measures on KNS ceramic powder samples by using two different set-ups: the reflection mode set-up and the transmission one. We have used a mode-locked Ti:Sapphire laser, with a wavelength output at $\lambda = 790\ nm$ and pulse duration $\tau = 120\ fs$.

3.1 Reflection mode set-up

The set-up we have realized to perform measures in reflection is shown in figure (3.1).

The light travels across the system formed by the half-wave plate and the polarizer: we weren't interested in a particular state of polarization, we used this system just because it let us change the power of incident radiation on the samples, by rotating the half-wave plate. We used a motorized mount to turn this device, in order to get many possible orientations of the half-wave plate.

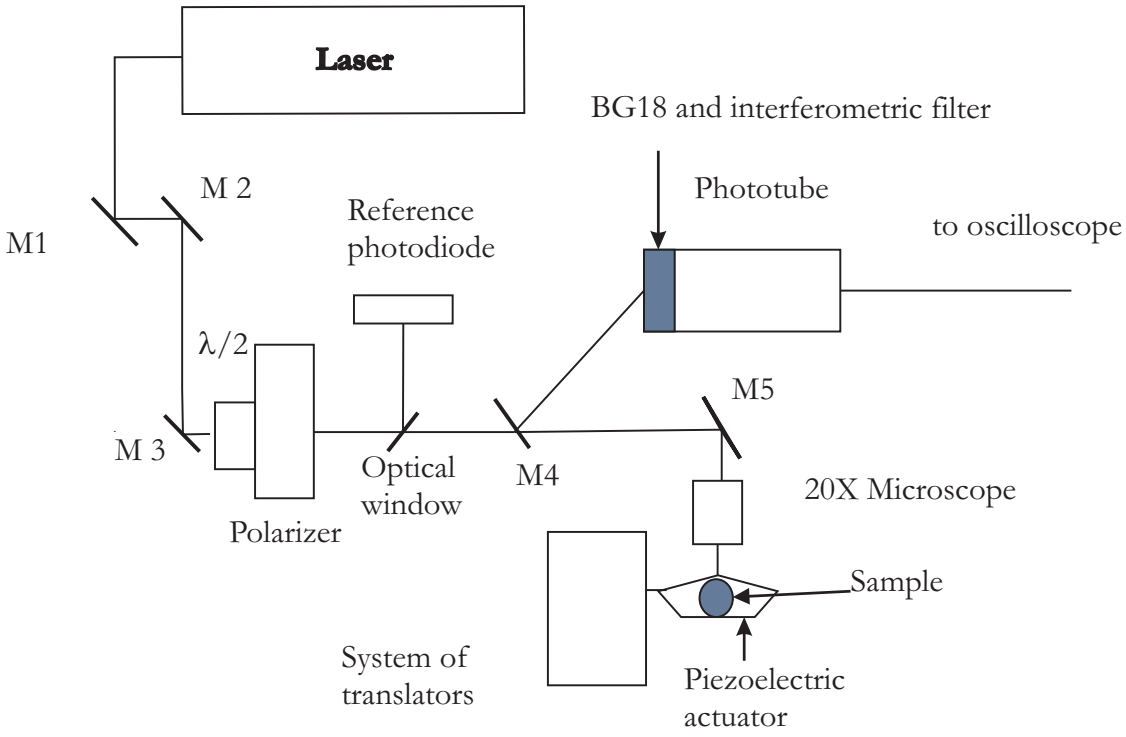

Figure 3.1: Reflection mode set-up

The optical window reflects only the 4% of the laser light towards a photodiode, used to have a signal reference. We shielded the photodiode with some neutral filters, to avoid the saturation of the detector and to keep it in the linear response regime.

The beam transmitted goes trough the M4 dichroic mirror (HR@400, HT@800) then is reflected by the M5 metallic mirror into the microscope 20X objective. The metallic mirror is a silver one, it can reflects any wavelength between $400nm - 2\mu m$.

Light enters the 20X Microscope to be focused on the KNS powder pressed on an optical window. We decided to use this devices as a support for our sample because of its transparency to any wavelength light.

The optical window was put on a piezoelectric actuator, supported by a system of two perpendicular translators and another controller: this mount let us to control horizontal translations, vertical translations and the tilt of the actuator. That's a main point of the setup: thanks to this fine regulations we were able to maximize the second harmonic intensity produced by the sample.

The second harmonic and the fundamental radiation goes back towards the M5 mirror, the metallic one, that can reflect both the wavelengths. The second harmonic is then reflected by the M4 mirror (HR@400, HT@800), while the fundamental is transmitted. The second harmonic impinges the phototube, by traveling across two blue bandpass filters (BG18) and an interferometric one.

The phototube was connected by a BNC coaxial cable to the oscilloscope (Tektronix TDS 3054).

The first operation we have done is the alignment of the set-up; by paying attention especially to the microscope. In this step we replaced the piezoelectric actuator with a metallic mirror, in order to have a reflected beam of fundamental radiation: we considered the alignment accomplished when the phototube saturated because of this beam. In fact the M4 mirror was supposed to transmit quite all the fundamental radiation, so the phototube could detect just a few of the pump also because of the BG18 and interferometric filters.

First we had to be sure that this set-up was able to detect a second harmonic signal; that's why we performed a non-linearity measure on a BBO crystal.

Non-linearity

We put the BBO at the working distance of the microscope, then we changed the intensity of the incident radiation by rotating the half-wave plate, and we measured the SHG signal. We repeated the same measure for one of our samples (KNS 23-27-50, $d < 32$). In both cases our goal was to find an evidence for the non-linear behavior of the samples. We plotted the second harmonic signal VS the incident intensity: we expected that a parabola would have fitted well the experimental data, as it happened.

Then we analyzed the second harmonic produced by three different ceramic glasses.

SHG (from ceramic glasses)

This measure was performed by using the reflection set-up except for one device: we replaced the piezoelectric actuator with a metallic mirror. We also have made a comparison with the data about KNS ceramic glasses analyzed in [1].

Then we performed the main measure of this work: we studied SHG from our samples, in order to make a determination of the coherence length.

Coherence length (from KNS powder)

We wanted to study the SHG from the different samples. We have carried this measure with the following technique: we put the powder on an optical window, the we pressed it with another optical window which was identical to the first. Then we removed the upper one and performed the measure.

3.1.1 **Laser system**

The laser-system is composed by three main elements: a diode-pumped laser (Coherent Verdi V10), a Ti:Sapphire oscillator (Mira 900) and the cavity dumper (APE Pulse Switch).

The laser Coherent Verdi V10 is the optical pump of the oscillator, it emits green radiation @532nm and has a maximum power of 10W, but we used it at 4W.

The femtosecond Ti:Sa oscillator Coherent Mira 900 is a mode-locked laser, which is capable of generating short laser pulses (120fs, @790nm) at a pulse repetition rate of 76MHz.

The Pulse Switch cavity dumper is used to reduce the repetition rate of the Mira 900 and to raise the pulse energy by several times: we had a pulse repetition rate of 54.3MHz, the maximum output power obtained for each pulse was 30mW. We got this value by setting the division rate at 100, when we had to perform measure we often set it at 50, in order to have more power.

The output beam has a spatial profile gaussian in shape. We were interested in the size of the laser beam spot, that's why we performed a knife-edge measurement. It consisted in "slicing" the laser light with a metallic blade and detecting the transmitted intensity. We fixed the blade to the piezoelectric actuator (see section 3.1.6), which was mounted on the system of translators (see figure 3.1).

We moved this device with the translators. We registered the position of the blade and the light transmitted, which was detected by the Thorlabs DET 210 photodiode (see section 3.1.2), so we built the spatial beam profile (figure 3.2).

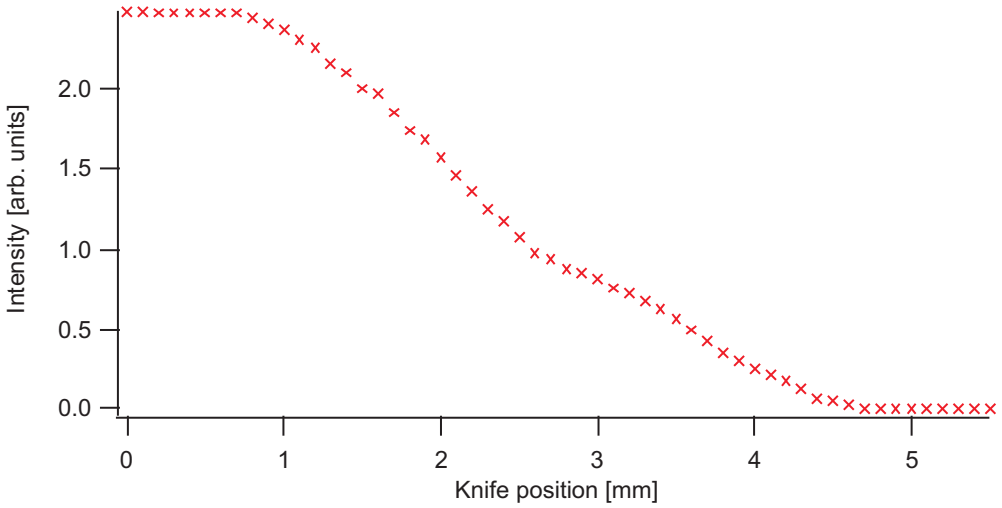

Figure 3.2: Beam profile

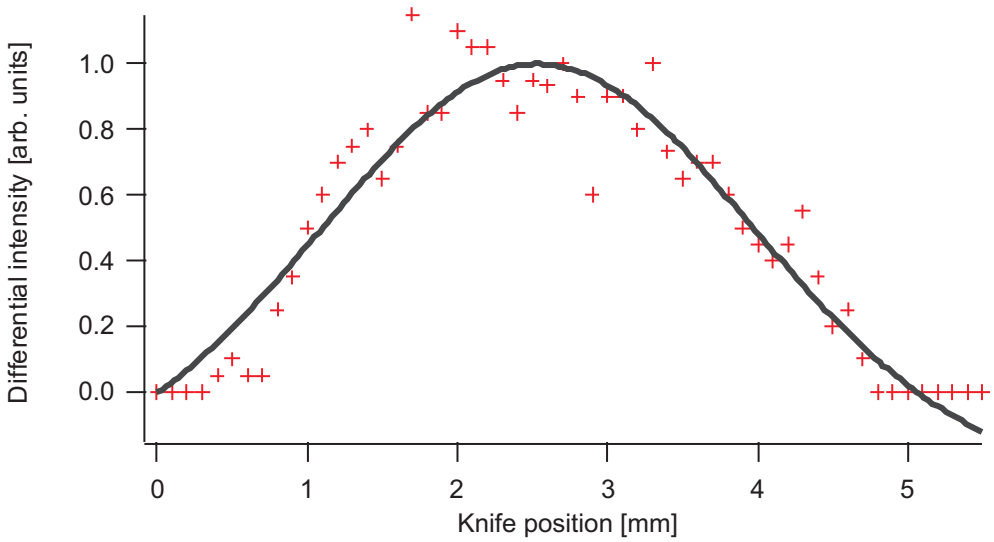

Figure 3.3: Beam profile fit with gaussian function

The beam profile of the spot is shown clearly in figure 3.3, which reports the derivative of the knife-edge profile vs the knife position. We fitted the differential intensity with a gaussian function whose FWHM is the width of our laser beam spot. We obtained the value $D = (3.3 \pm 0.5)mm$.

This result is very useful in order to know the spot size of the laser beam when it is focused by different devices (see section 3.1.5 and 3.2.1).

Another important feature of the laser beam is the energy content of each pulse; it is given as:

$$E_p = (\text{Power meter signal in W})/R_r \tag{3.1}$$

where R_r is the repetition rate of the laser. The peak intensity can be obtained from the following relation

$$I_p = \frac{E_p}{A \cdot \tau} \tag{3.2}$$

where τ is the life-time of each pulse and A is the area on the sample. We evaluated the area of the beam in the focus of a microscope (reflection set-up) and an achromatic doublet (transmission set-up).

3.1.2 **Photodiode**

The reference photodiode we used was a Thorlabs DET210 one. It is a silicon PIN photodiode featured by a very little active area ($0.8mm^2$), which is the only part of the detector that interacts with radiation. The damage threshold is $100mW$ in continuous wave (CW) and $0.5J/cm^2$ for $10ns$ pulsed wave.

The maximum of the photodiode's response curve is about our fundamental wavelength ($\approx 800nm$), the responsivity (Re(λ))is about 0.4 A/W in this spectral region (see figure (3.5)). The responsivity is a useful data to give an estimation of the photocurrent expected, which is converted in voltage (in order to view it on an oscilloscope) by adding an external load resistance (R_{load}).

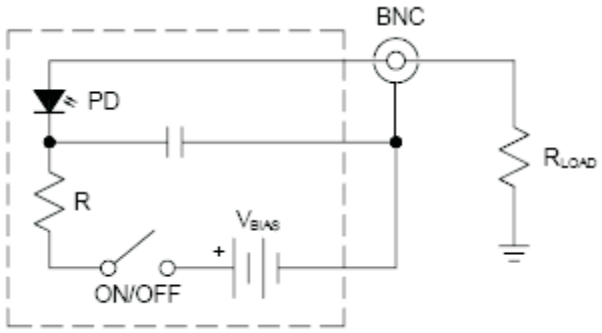

Figure 3.4: Structure of Thorlabs DET210 photodiode

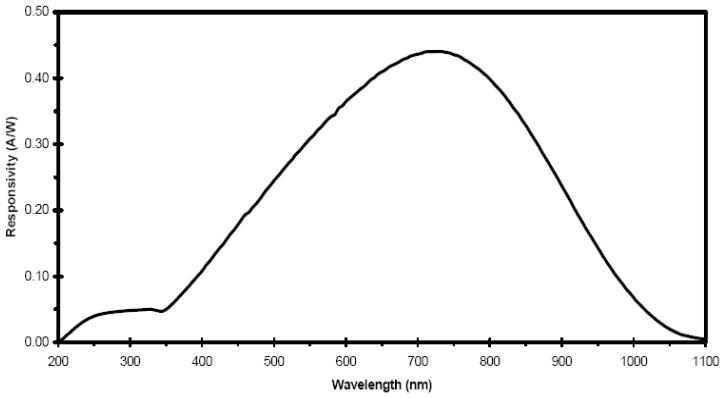

Figure 3.5: Spectral response of Thorlabs DET210 photodiode

The output voltage is

$$V_o = \mathrm{Re}(\lambda) \cdot P \cdot R_{load}$$

where P stays for the power of the incoming radiation on the photodiode.

Besides we are able to value the bandwidth (f_{bw}) and the rise-time response (t_r), that depend on the capacitance of the DET210 (C_j) and on the load resistance; in fact the relationship that holds is

$$f_{bw} = \frac{1}{2\pi C_j R_{load}}$$

$$t_r = \frac{0.35}{f_{bw}}$$

We wired the photodiode to the oscilloscope with a BNC coaxial cable. First we set the input impedance of the oscilloscope on 50Ω, so we could see that the light pulse was detected by the photodiode. Later we change the impedance to the value of $1M\Omega$, with the aim to slow the time response of the photodiode: in fact this device can be thought as a RC circuit with a relaxation time $\tau = RC$. Our intent to increase the value of τ is due to the need for an integration of the signal over a longer time range; if we set 50Ω as impedance we can't see any signal except for the narrow time window of the pulse. So we could see a continuous signal on the oscilloscope, which was the result of an integration over the peaked signals corresponding to many incoming light pulses on the photodiode.

We had to screen the photodiode with some neutral filters, to avoid its saturation and to keep it in his linear response regime.

3.1.3 **Photomultiplier (Phototube)**

A photomultiplier is a device which converts light into a measurable electric current. It is so sensitive that it can be used to perform photon counting measure, because it can detect a single photon. We used an Hamamatsu R7518P with a C6270 socket supply.

Figure (3.6) shows a schematic diagram of a photomultiplier.

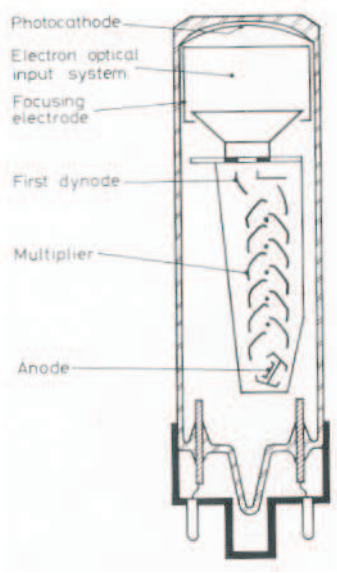

Figure 3.6: Schematic representation of a photomultiplier

It consists of a cathode made of photosensitive material followed by an electron collection system, an electron multiplier section (or dynode string) and finally an anode from which the final signal can be taken. All parts are housed in an evacuated glass tube.

When the photomultiplier is in function, a voltage is applied to the cathode, dynodes and anode such a potential "ladder" is set up along the length of the cathode-dynode-anode structure. When an incident photon interacts with the photocathode, an electron is emitted via photoelectric effect. Because of the applied voltage the electron is then directed and accelerated towards the first dynode, where it transfers some of its energy to the dynode's electrons. This involves emission of secondary electrons, which are accelerated towards the next dynode where more electrons are released and further are accelerated.

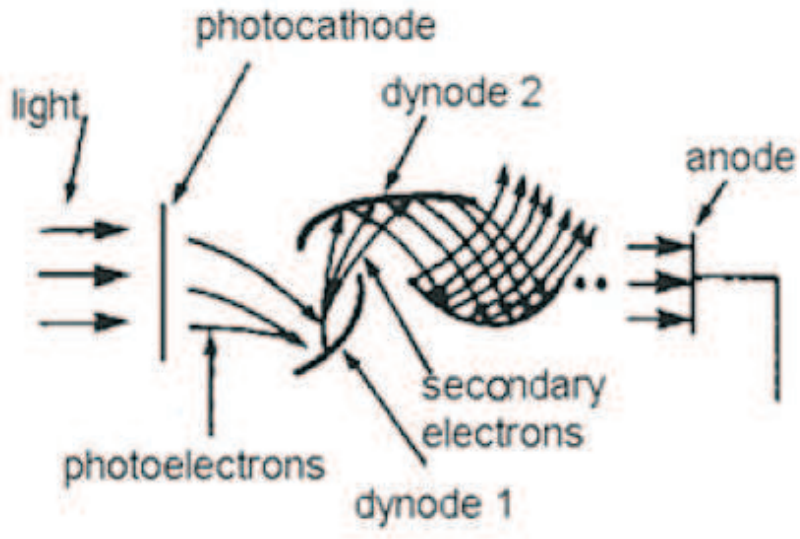

Figure 3.7: Electron multiplier section of a phototube

As a result an electron cascade is created down the dynode string, as can be seen in figure (3.7). This cascade is collected to give a current which can be amplified and analyzed.

Photomultipliers may be operated in continuous mode (i.e. under a constant illumination) or in pulsed mode. In either mode the current at the output will be directly proportional to the number of incident photons. The photomultiplier we used in pulse mode is able to detect even ultra-short pulses: in fact we had $120fs$ pulses, while the time response of the R7158P is of the order of ns.

We have to take in consideration some features of a phototube, to describe it properly. We have seen that the photocathode converts incident light into a current of electrons by the photoelectric effect. That's why the photocathode usually is made of semiconductors or multi-alkali compounds (for example GaAs or InGaAs), in fact these materials are featured by a low

work function. As it's well known, photoelectric effect has a threshold; i.e. a certain minimum frequency of the incoming radiation is required to make it take place. Above this threshold, however, the photoemission probability is less than 100%: the efficiency for photoelectric conversion depends on the frequency of the incoming light and on the structure of the material.

This spectral response is expressed by the *quantum efficiency* $\eta(\lambda)$

$$\eta(\lambda) = \frac{number\ of\ photoelectrons\ released}{number\ of\ incident\ photons\ on\ cathode(\lambda)}$$

where λ is the wavelength of the incident light. An equivalent quantity is the *cathode radiant sensitivity*, which is defined as

$$S(\lambda) = \frac{I_k}{P(\lambda)}$$

where I_k is the photoelectric emission current and $P(\lambda)$ is the incoming radiant power. $S(\lambda)$ is usually given in units of ampere/watts and it can be related to the quantum efficiency by

$$S(\lambda) = \frac{e\lambda\eta(\lambda)}{hc}$$

where e is the electron charge and c is the light's speed.

Figure (3.8) represents the quantum efficiency and the cathode radiant sensitive in function of the wavelength. It must be noted that the peak of the quantum efficiency is at $400nm$, which is the wavelength of the second harmonic signal we had to detect.

The photocurrent is amplified by the dynodes, which are secondary emission electrodes.

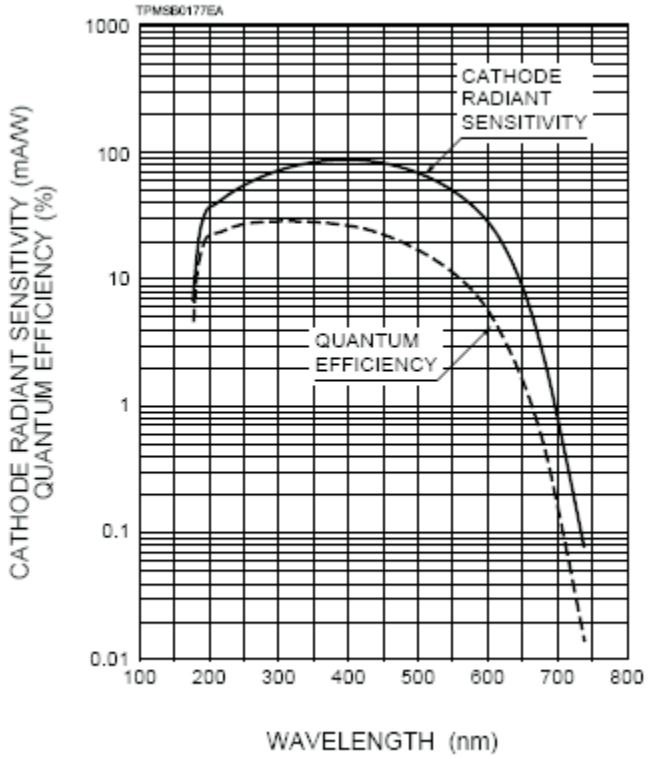

Figure 3.8: Hamamatsu R7518P spectral response

The gain of each dynode is known as *secondary emission factor,* δ. Dynodes are made of CsSb, because it has a very high secondary emission factor and a low thermionic emission (i.e. low noise).

The overall gain of a photomultiplier depends on the number of dynodes and on the secondary emission factor δ, which is a function of the energy of the incident electrons.

This energy is obviously related to the potential difference V_d between the dynodes, so we can write

$$\delta = KV_d$$

where K is a proportionality constant. If we assume that V_d has the same value for every dynode, the overall gain can be expressed as

$$G = \delta^n = (KV_d)^n \tag{3.3}$$

where n is the number of the dynodes. From (3.3) it is possible to calculate the number of dynodes n, required to get a certain gain G with a minimum supply voltage V_s

$$V_s = nV_d = \frac{nG^{1/n}}{K}$$

Minimizing we find,

$$\frac{dV_s}{dn} = \frac{1}{G^{1/n}} - \frac{n}{K}\frac{G^{1/n}}{n^2}\ln G = 0, \quad n = \ln G$$

This is a useful result, because operating at minimum voltage could be desirable from the point of view of noise.

Another important relation is the variation in gain with respect to supply voltage. From (3.3) we calculate

$$\frac{dG}{G} = n\frac{dV_d}{V_d} = n\frac{dV_s}{V_s}$$

which means that to keep a gain stability of 1%, the voltage supply must be regulated to within 0.1%.

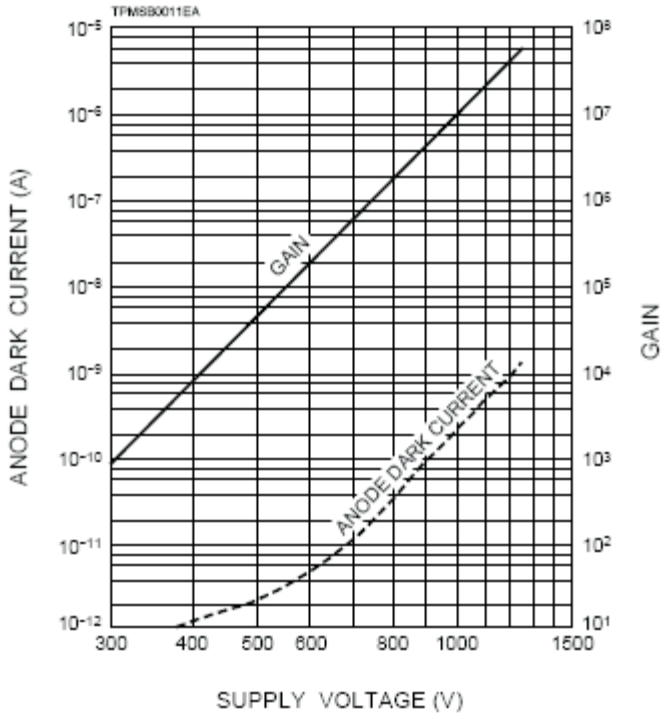

Figure 3.9: Hamamatsu R7518P gain

The dependance of the gain from the supply voltage for our phototube is shown in figure (3.9).

The device was connected to the oscilloscope by a BNC coaxial cable. We set the input impedance of the oscilloscope on $1M\Omega$, so we could read the current generated by the phototube as a voltage. To minimize the noise's influence, we averaged the signal over a temporal window. Laboratory's lights could damage permanently the dynodes, so it was fundamental to work in a dark environment.

We screened the photodiode with two BG18 and an interferometric filters, in order to cut the fundamental frequency and transmit only the second harmonic.

3.1.4 **Filters**

We used three kinds of filters: bandpass filters, attenuation filters and interferometric filter. We put two BG18 bandpass filters before the phototube to cut the fundamental radiation, so the signal detected by the photomultiplier should have been only second harmonic.

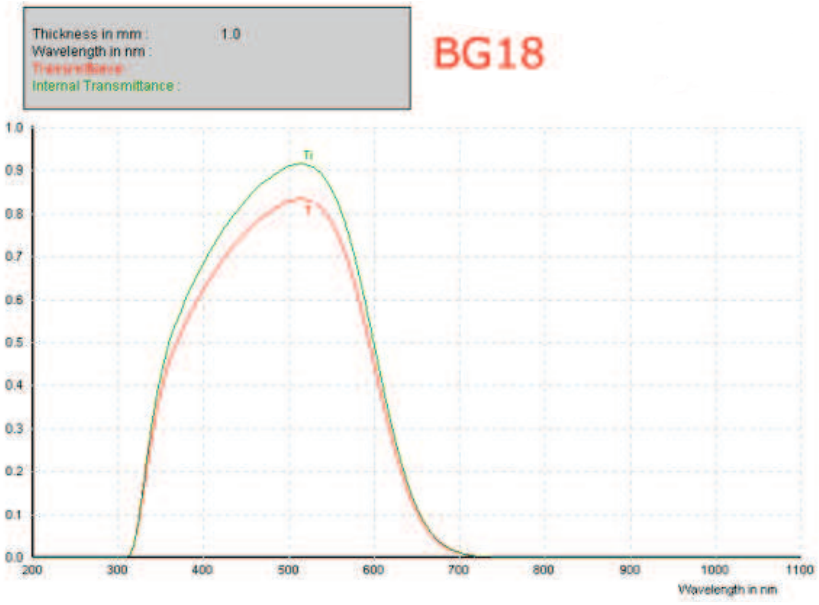

Figure 3.10: BG18 transmission

The transmittance of BG18 filters is represented in fig 3.10: it should be noticed that for the wavelength $\lambda = 790\ nm$ (the one we had to cut) the BG18's transmittance is $9 \cdot 10^{-5}$, meanwhile for $\lambda = 400\ nm$ (the one we wanted to detect) T is 0.62. The ratio of these two values of transmittance is

about 10^5, that's why we used this filter. The transmittance's peak is about @500 nm.

We used also the attenuation filters NG5 and NG11 to screen the reference photodiode, to avoid its saturation.

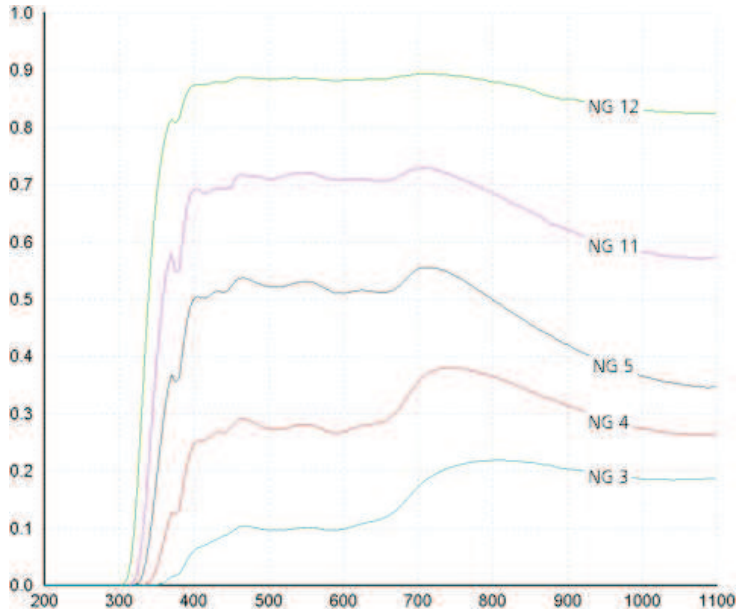

Figure 3.11: NG11 and NG5 transmission

Figure 3.11 shows the transmittance of NG5 and NG11 filters: the former transmits 0.50 at @790 nm, the latter 0.69.

We used also an interferometric filter at @400 nm, put on the window of the phototube's photocathode to cut further the fundamental radiation.

3.1.5 **Microscope**

We used a Newport M-20X microscope to focus the laser beam on the sample and then, once the sample had produced second harmonic, to collect the reflected signal. The working distance of this device is 1.7 mm.

By using the gaussian beams propagation theory, it is possible to calculate the depth of focus and the spot diameter.

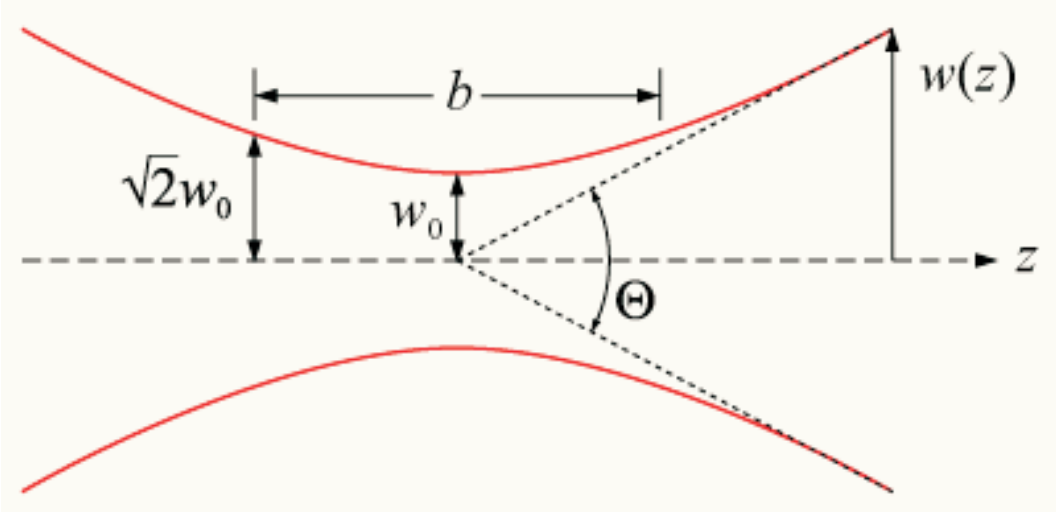

Figure 3.12: Gaussian beam's propagation

Look at the fig 3.12: the spot size is a function of z (which is the propagation direction), $\omega(z)$. The minimum of this function ω_0 is called *waist*.

For a beam of wavelength λ at a distance z along the beam from the beam waist, the variation of the spot size is given by

$$\omega(z) = \omega_0 \sqrt{1 + \frac{z}{z_0}}$$

where the origin of the z-axis is defined, without loss of generality, to coincide with the beam waist, and where

$$z_0 = \frac{\pi \omega_0^2}{\lambda}$$

is called the *Rayleigh range*. So at a distance from the waist equal to the Rayleigh range z_0, the width ω of the beam is

$$\omega(\pm z_0) = \omega_0\sqrt{2}$$

The distance between these two points is called the *confocal parameter* or *depth of focus* of the beam:

$$b = 2z_0 = 2\frac{\pi\omega_0^2}{\lambda}$$

The spot diameter in the focus is expressed as

$$d_0 = 2\omega_0 = \frac{2\lambda f}{\pi D} \tag{3.4}$$

where f is the focal length of the microscope and D is the spot diameter before the microscope. We obtained the value $D = (3.3 \pm 0.3)mm$ with knife-edge technique described in section 3.1.1.

By applying the equation (3.4) we found that in the focus of the microscope the spot diameter should be $d_0 = (1.5 \pm 0.5)\mu m$; we performed a knife-edge measurement in the focus of the microscope to verify this result. We wanted to detect a spot size in the order of micron, so we had to modify the measure technique. We moved the blade by moving piezoelectric actuator controlled by its interface, that let us to realize displacements in $1\mu m$ steps.

According to the equation 3.1.5 the focus depth of our system is $b = 2z_0 = (5 \pm 1)\mu m$.

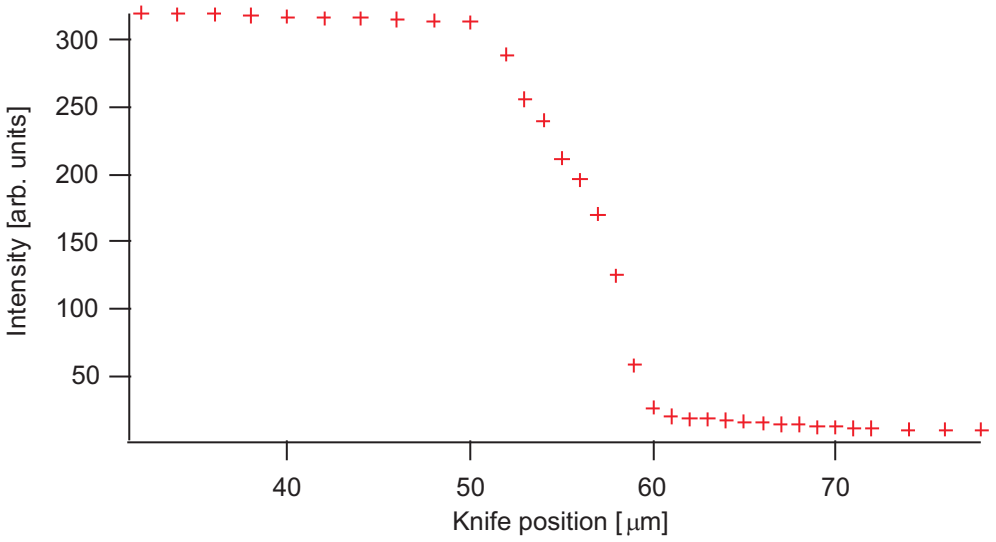

Figure 3.13: Beam profile

We reported the spatial beam profile in figure (3.13).

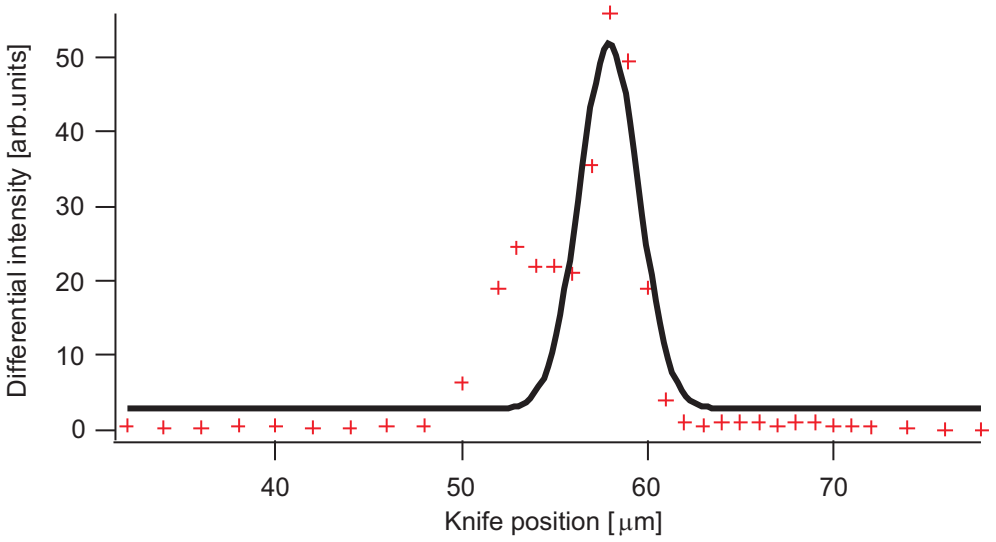

Figure 3.14: Beam profile fit with gaussian function

The graph that shows the derivative of the knife-edge profile vs the knife position is figure (3.14).

The value of the FWHM, so the spot size in the focus of the microscope, is $d_0 = (3.5 \pm 0.5)\mu m$.

3.1.6 **Piezoelectric actuator**

We used a Piezosystem jena NV40/1CL piezoelectric actuator: it is a device for moving a mechanism via inverse piezoelectric effect. This is a typical effect of some materials (mainly crystals and certain ceramics): when exposed to an electric field they lengthened or shortened according to the polarity of the field, and in proportion to the strength of the field. The direct piezoelectric effect occurs when these materials are subjected to a mechanical force, in this situation they become electrically polarized.

The NV40/1CL has a maximum displacement of 300 μm. We chose to use it to solve a problem linked to the spot size: the 20X microscopy focus the beam in a spot smaller than the single grain of our samples. That means the signal we detected was influenced by the geometry of the single grain, and by the part we hit with the fundamental radiation (zones near edges produce more SH than flat ones). The piezoelectric actuator allowed us to make an average measure on more grains: we put the sample on the device, then we applied an oscillatory signal (produced by a functions generator) to the actuator, hence it moved forward-and-back by making us collect an average signal.

3.2 Transmission mode set-up

The measures in transmission required to change the set-up.

As you can see in figure (3.15) the differences between this set-up and the reflection one are all after the optical window.

The fundamental radiation is focused by the achromatic doublet on the sample. We put the powder on an aspheric lens, which is placed in a mount (we'll call it MJ23), it was machined and realized specifically for this work.

The MJ23 mount is composed by two elements: the first one is round in shape, the aspheric lens was screwed within it. This item stayed on the second element of the MJ23 mount. The second piece is made of black PVC, it has the place to insert the BG18 and the interferometric filters. This piece was siliconized directly on the phototube.

We'll describe just the devices which didn't appear in the former set-up.

3.2.1 Achromatic doublet

The achromatic doublet was aimed to focus the fundamental radiation on the sample. This device has a diameter of $25.4mm$ and a $20cm$ focal length, besides it is anti-reflection coated for the spectral range $650 - 1050nm$.

An achromatic doublet is used to correct the chromatic aberration (i.e. different wavelength radiation are focused in different places by the same lens), as can be seen in figure (3.16). Our source is not perfectly monochromatic, each pulse is peaked on the value 790 nm, but it has a little wider spectral content: that's why we used the achromatic doublet.

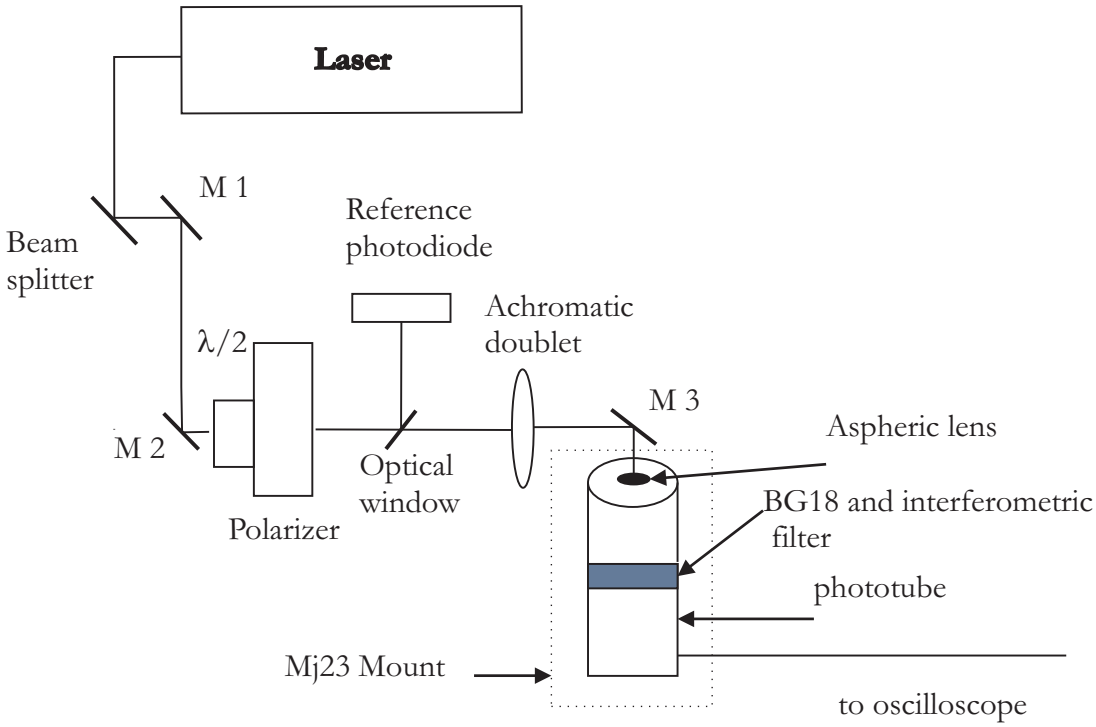

Figure 3.15: Transmission mode set-up

By applying equation (3.4) we got the value of the laser beam spot size in the focus of the achromatic doublet, $d_0 = (30 \pm 10)\mu m$. We performed a knife-edge measurement to check this value; we used exactly the same technique we had used with the microscope (see section 3.1.5). We have carried out the measure twice, se we have two runs of data.

We reported the beam profile and the derivative of the knife-edge profile vs knife position in figure (3.17) and (3.18).

The spot size obtained from figure (3.18) is $d_0 = (30 \pm 2)\mu m$.

The second run data are reported in figure (3.19), we reported only the graph with the gaussian fit.

The spot size calculated from figure (3.19) is $d_0 = (30 \pm 1)\mu m$. Hence the

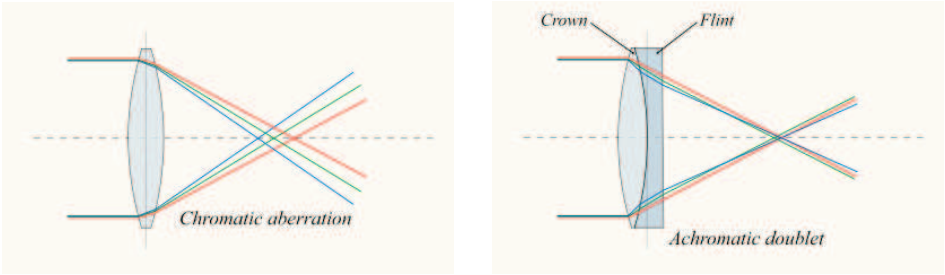

Figure 3.16: Achromatic doublet correction of chromatic aberration

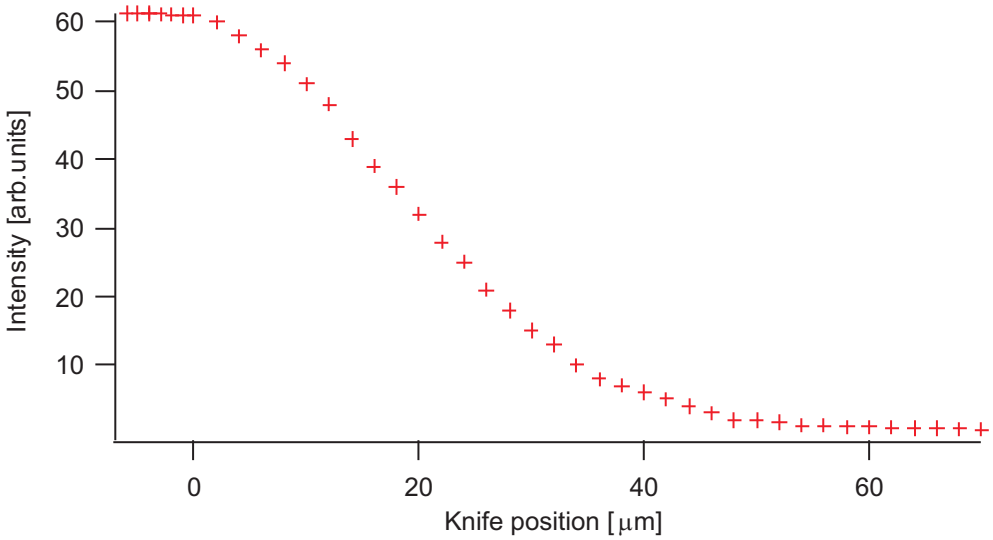

Figure 3.17: First run beam profile

experimental data agree with the theoretic forecast.

From the equation (3.1.5) it follows that the depth of focus of the achromatic doublet is $b = 2z_0 = (2 \pm 0.2)mm$.

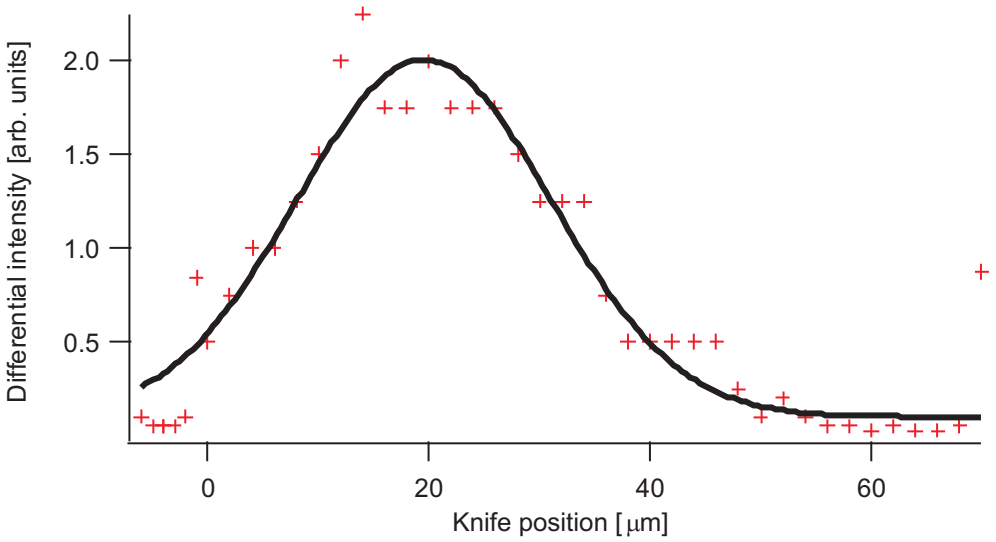

Figure 3.18: First run beam profile fit with gaussian function

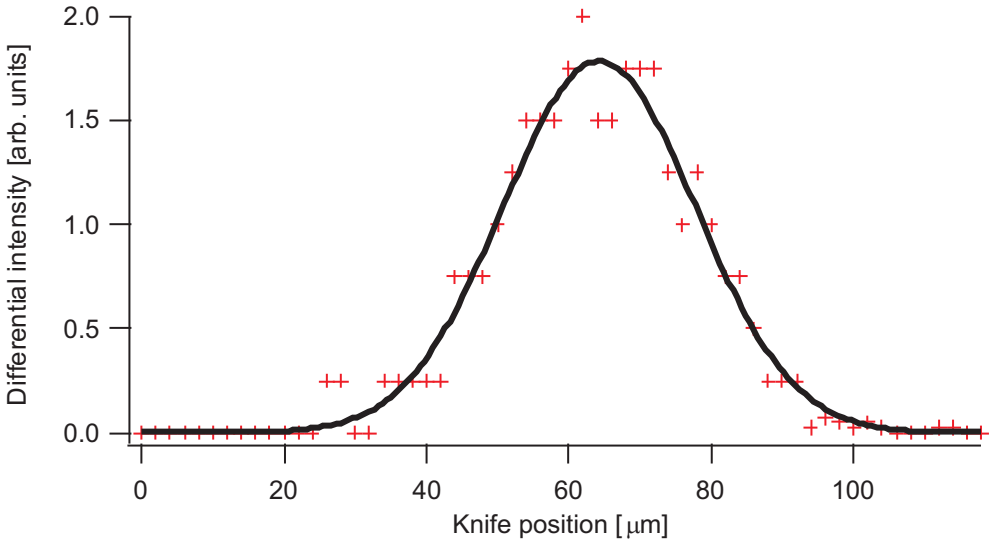

Figure 3.19: Second run beam profile fit with gaussian function

3.2.2 **Aspheric lens**

An aspheric lens is a device used to correct the spherical aberration, that occurs because of the spherical surface of the lens, as we can see in figure (3.20).

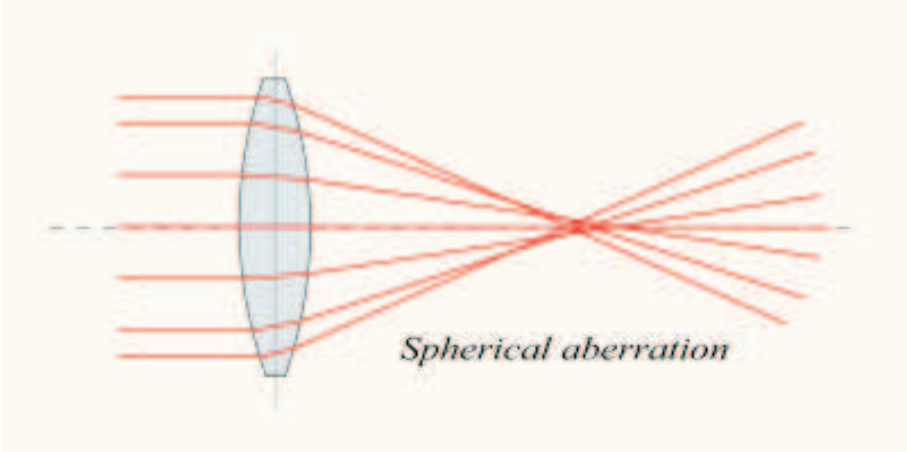

Figure 3.20: Spherical Aberration

Hence thanks to the achromatic doublet and to the aspheric lens, aberrations weren't supposed to influence our measure.

The aspheric lens played the leading role in the transmission set-up, in fact if satisfied many requests:

- we used it as powder-container for our sample;
- refractive index of the lens's glass (C0550) doesn't significantly change for our two work-wavelengths. In fact $n = 1.62 \quad$ for $\lambda = 400\ nm$ and $n = 1.59 \quad$ for $\lambda = 790\ nm$;
- its focal length is very short ($f = 1.1\ mm$)

We needed a focal length as short as possible, because the powders were in contact with the lens surface. So we had to minimize the distance between the second harmonic source (powders) and the lens's focus, in order to get a parallel beam.

4. Measurements

We performed three different kinds of measurements: non-linearity, SHG from ceramic glasses, coherence length of KNS powder.

4.1 Non-linearity

The non-linearity measurement was performed with two samples: a BBO crystal and KNS powder $23 - 27 - 50$, $d < 32$. Both these measures were performed with the reflection mode set-up.

The first step was carried out just to get sure that our set-up was able to detect a second harmonic (SH) signal; so we use a BBO as calibrator.

We replaced the piezoelectric actuator with the nonlinear crystal then, after we had checked the alignment of the set-up, we performed the measure with the following technique: we collected the data of the second harmonic signals (from the phototube) and the incoming reference intensity (from the reference photodiode). Hence we moved via software the motorized mount of the half wave plate, in order to change the intensity of the incoming radiation

and then we collected the data again.

Our goal was verify the following relation

$$I(2\omega) \propto I^2(\omega)$$

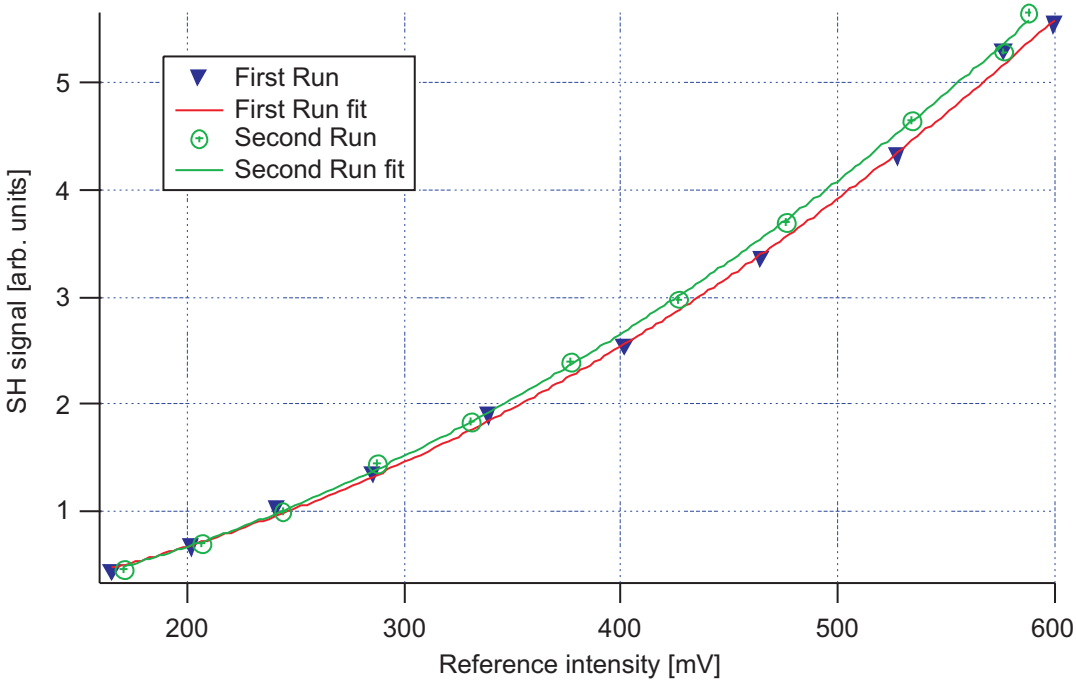

Figure 4.1: BBO non-linearity

By plotting the SH vs the incident power we expected that the experimental data could be well fitted by a parabola, as can be seen in figure (4.1). The fit function is

$$y = y_0 + A\ x^n$$

We measured the data into two different runs of ten points each one.

Run	Fit coefficient
1	2 ± 0.1
2	1.9 ± 0.1
1 + 2	1.9 ± 0.1

Table 4.1: Fit coefficients

We reported the fit coefficients for the different runs in table (4.1), where we also considered the fit of the two runs together. Anyway the value of the fit coefficient doesn't noticeably change.

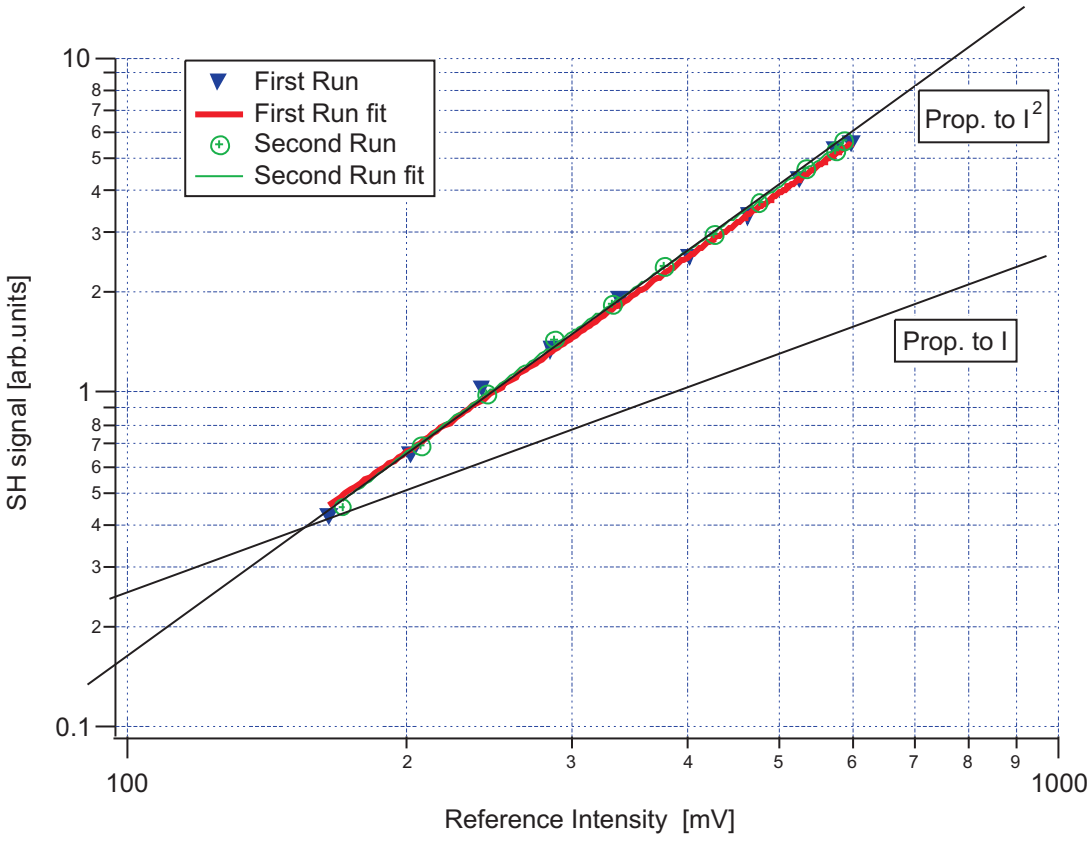

Figure 4.2: BBO log scale non-linearity

We change the plot scales into logarithmic ones, in order to show clearly the non-linear behavior of the BBO crystal (see figure (4.2)). In fact if $y \propto x^n$ (as in our case) by using the logarithmic scale we have on the abscissa $\log x^n = n \log x$ and on the ordinates $\log y \propto n \log x$, that is a linear relation. Figure (4.2) shows an evidence for the non-linear behavior of the BBO crystal.

We repeated the same measurement, with the same technique on one of the KNS powder samples: we used the KNS $23 - 27 - 50$, $d < 32$. In this step the powder was just spread (not pressed) on the surface of a metallic (Al) mirror, that replaced the BBO.

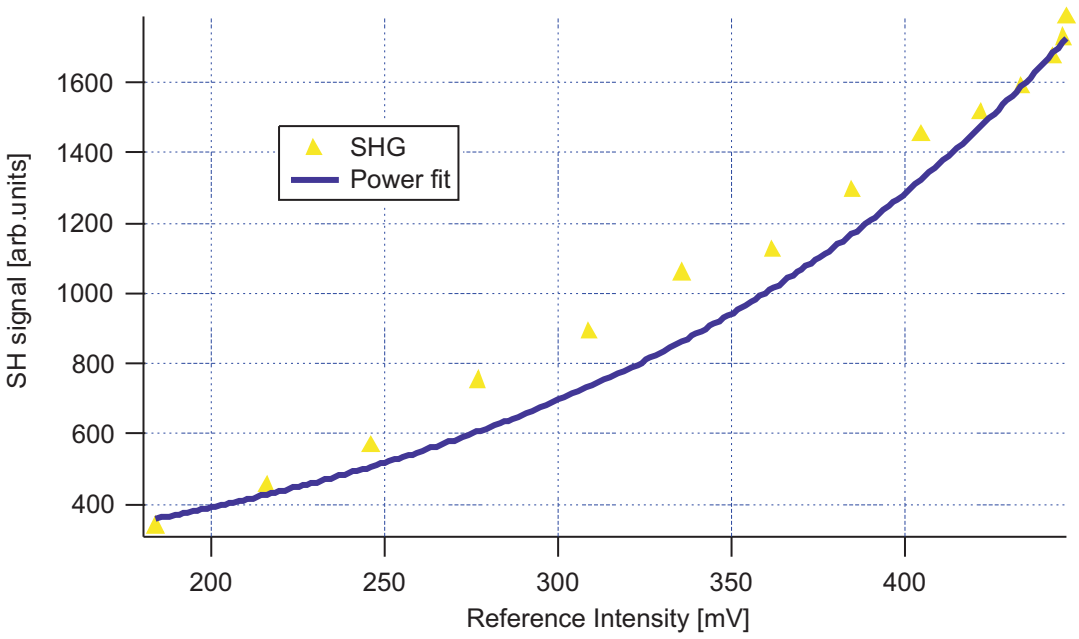

Figure 4.3: KNS non-linearity

Data are shown in figure (4.3), the fit gives $n = 1.9 \pm 0.2$.

By looking at the logarithmic plot in figure (4.4), it is clear that also this time the sample has a non-linear response.

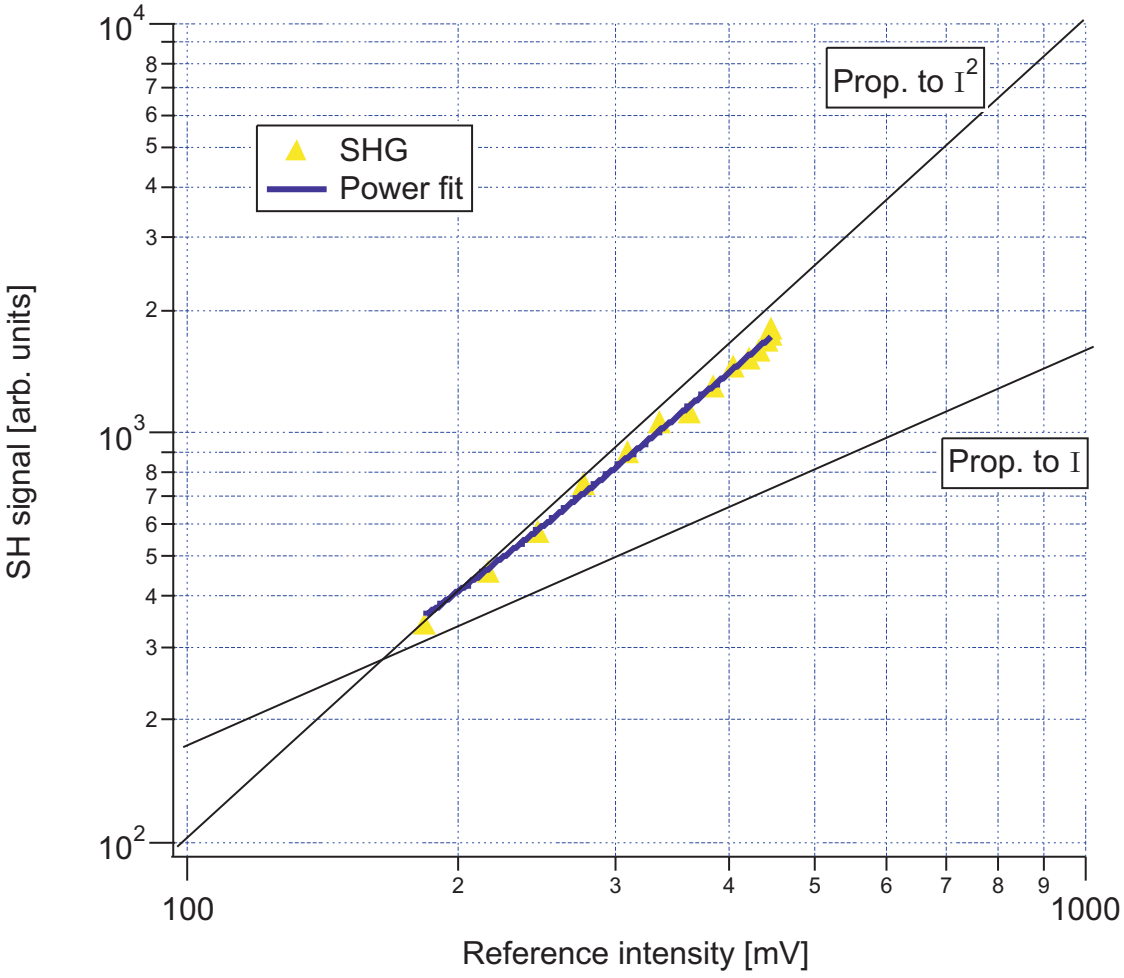

Figure 4.4: KNS log scale non-linearity

We had some difficulties in carrying out this measurement, because of the small second harmonic intensity produced by the sample. Besides we hadn't yet replaced the metallic mirror with the piezoelectric actuator: it is a device that let us acquire a signal averaged on more grains, despite of the spot size (see section 3.1.6). Another problem dealt with the powder on the mirror: it was just spread on the optical device without being pressed. It means that there could be layers different in thickness and with a different surface

configuration; this could involve some changes in SH signal depending on the zone we were hitting with the laser beam.

4.2 SHG from ceramic glasses

The second set of measurements consisted in detecting second harmonic generation from three ceramic glasses: NaNs, LiKNS, KNaNs, all these samples are as-quenched. The aim of this part of work consisted in establishing wether this samples had an improved SHG efficiency, with respect the KNS ceramic glasses (subjected to an annealing process) previously produced and studied.

The KNS ceramic glasses was the subject of [1]; we used the most performing sample analyzed in this work in order to make a comparison.

In fact Dott. Bignardi was able to determine the efficiency of KNS ceramic glasses, by a comparison with the efficiency of an out-of-phase-matching BBO.

We couldn't find a quantitative value of ceramic glasses' efficiency, because we didn't have a reference (like the BBO in [1]). We can only compare the glasses's efficiency among themselves, that's why we used one of Dott.Bignardi's samples as a reference.

We chose to use the best sample analyzed in [1], KNS 23-27-50 2h 680°C.

We report the main result of [1] in figure (4.5): KNS can produce SH with an efficiency 10^{-5} times a BBO.

We performed this measurement with the reflection mode set-up. We put the ceramic glasses on the metallic mirror, then we focused the laser beam by using the vertical translator.

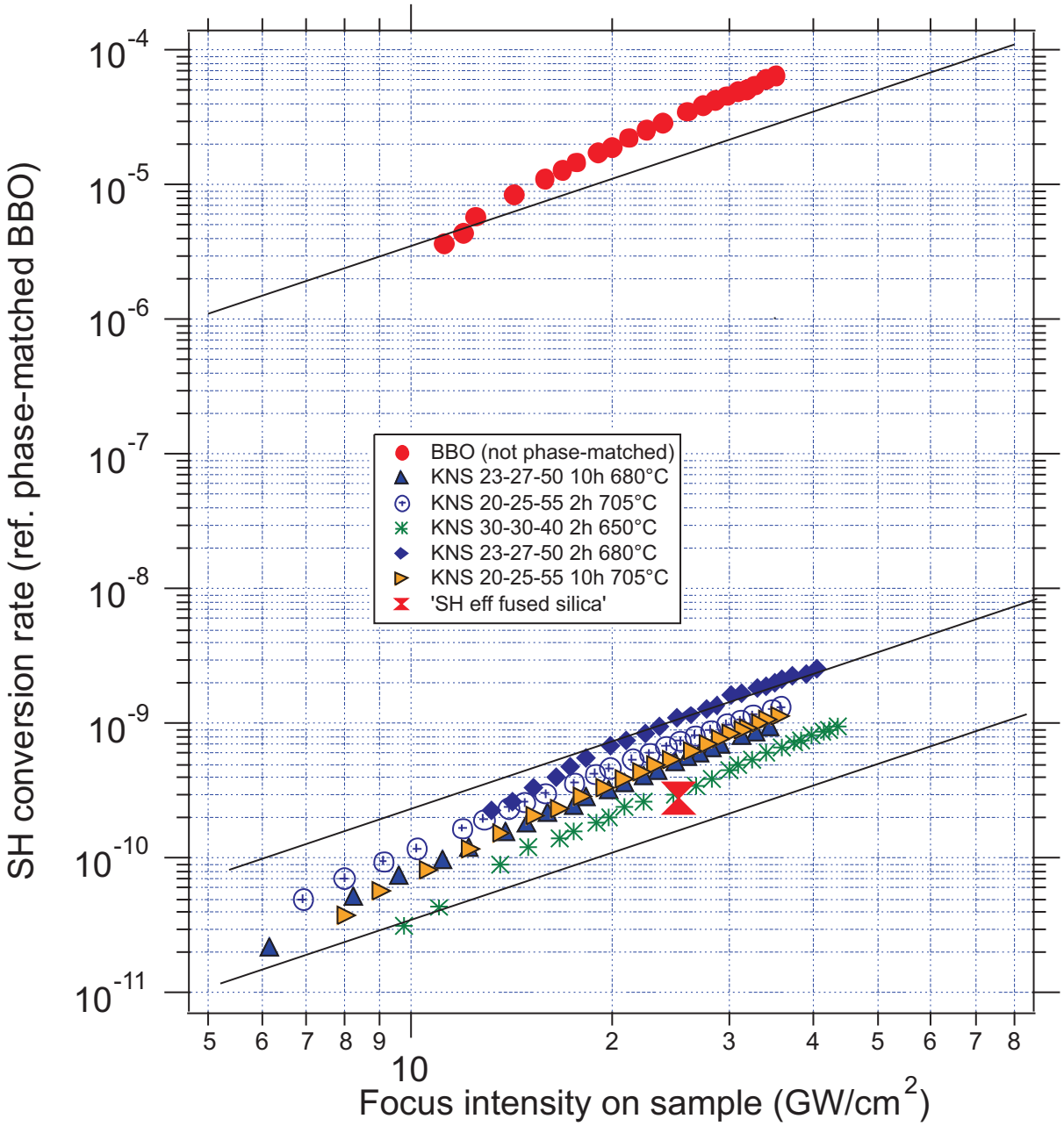

Figure 4.5: SHG efficiency in KNS glasses and BBO crystal, with detection range of the employed devices

When the sample was at the microscope's working distance it was possible to see a blue spot on the ceramic glass: that's an evidence for the second harmonic generation process. Hence we noticed something interesting: by scanning horizontally (using the translator) the samples, the phototube detected different signals. It means that the glasses showed lack of homogeneity; that's why we chose to measure a second harmonic signal averaged on ten different points of the sample.

We had to face another problem: the measurement took us enough time to let the incident power change significantly. We could notice it by reading the values detected by the reference photodiode, that's why we normalized the second harmonic signal. This means that we divided the SH intensity by the square of the incident reference intensity.

We took also note about the offset (due to noise), it significantly influenced our data because the ceramic glasses produced a very few second harmonic intensity. So we subtracted the offset to the second harmonic signal before normalizing it. We averaged the normalized value of the second harmonic intensity.

We needed to know the focus intensity of our laser beam on the sample, in order to use the calibration of KNS shown in figure (4.5). It's useful to recall equations (3.1) and (3.2), which allow us to calculate the peak intensity of each pulse

$$E_p = (\text{Power meter signal in W})/R_r \tag{4.1}$$

$$I_p = \frac{E_p}{A \cdot \tau} \tag{4.2}$$

The area of the beam in the focus is obtained by the relation $A = pir^2$, where r is half of the spot diameter. In our case we got

$$E_p = \frac{56mW}{54MHz} = 1 \cdot 10^{-9}J = 1nJ \tag{4.3}$$

$$I_p = \frac{1nJ}{\pi(1.75 \cdot 10^{-6})^2 m^2 \cdot \ 120 \cdot 10^{-15}s} = 80 \ GW/cm^2 \tag{4.4}$$

So we can evaluate the conversion rate of the KNS ceramic glasses, by watching the value of the conversion rate relative to the focus intensity of 80 GW/cm^2 in figure (4.5), the conversion rate is $8 \cdot 10^{-9}$. Hence we put the measured value of second harmonic intensity of the KNS equal to one, and scaled the data relative to the other glasses; so we had an estimation of the conversion rate value for all the samples.

Sample	**SHG (scaled)**	**Conversion rate**
KNS	1	$8 \cdot 10^{-9}$
KNaNS	0.9	$7 \cdot 10^{-9}$
LiKNS	1.2	$1 \cdot 10^{-8}$
NaNS	0.9	$7 \cdot 10^{-9}$

Table 4.2: SHG from ceramic glasses

Results are reported in table (4.2): only the LiKNS sample is able to produces more second harmonic than the KNS one.

4.3 Coherence length (from KNS powder)

This third measure was the main goal of this work: analyzing the second harmonic intensity in function of the KNS powder grain size.

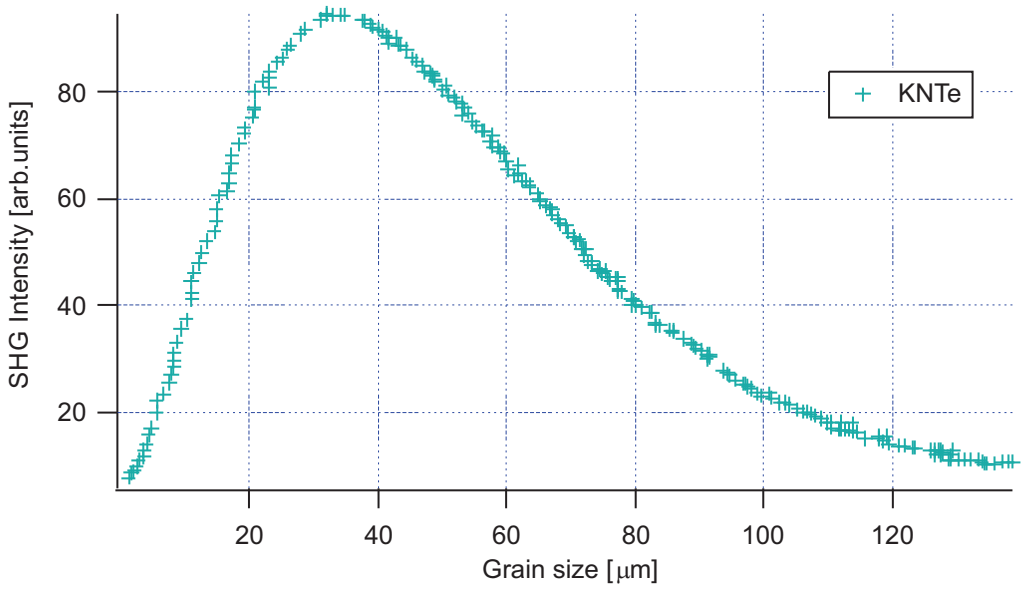

Figure 4.6: Comparison plot

We found in literature a work made on different samples (SHG from KNTe powders), but with the same measure we performed. We used the plot in figure (4.6) as a comparison, we took it from [2].

Four samples were available:

- KNS $23-27-50,\ d<32\mu m$ as-quenched;
- KNS $23-27-50,\ 32<d<45\mu m$ as-quenched;
- KNS $23-27-50,\ 45<d<90\mu m$ as-quenched;
- KNS $23-27-50,\ 90<d<125\mu m$ as-quenched;

Hence we could get four points in the plot.

We were interested in finding the peak of the plot, in order to give an estimation of the coherence length of the KNS.

We performed the measure in two different ways: by using the reflection mode set-up and the transmission one.

4.3.1 **Reflection measure**

The first attempt we did with the reflection set-up (see section 3.1, figure (3.1)) gave bad results.

We put the powder spread on the metallic mirror, like we had done in the non-linearity measure. Unlike the ceramic glasses, when the sample was at the working distance of the microscope, no blue spot could be seen. Besides we noticed strong differences in SH intensity, by moving the horizontal translator. This happened because there were zones with different powder layers' thickness; a bigger amount of powder means much more scattering, so in these zones the second harmonic intensity vanished.

Another problem dealt with the spot size: the 20X microscope focus the beam in a spot smaller than the single grain of each our samples. So the signal detected by the phototube was influenced by the geometry of the single grain, and also by the part we hit with the laser beam (zones near edges produce more SH than flat ones).

We tried to overcome these troubles by measuring an averaged signal. So we collected data by hitting with laser different zones of the powder (we moved the metallic mirror with the translators) and then we averaged these data.

The measure failed, because we detected an intensity trend different from the one in figure (4.6). In our opinion the causes are those just explained previously: spot size and powder's lack of homogeneity. Besides this technique has another drawback, that is it's not repeatable, in fact every time someone would try to perform the measure, the powder's layer on the mirror would always be inevitably different.

Thus we taught how to improve the set-up and the measure technique.

As far as the set-up is concerned, we replaced the metallic mirror with the piezoelectric actuator. This device let us to solve the problem relative to the spot size; in fact it moved forward-and-back in a displacement range of less than $300\mu m$ via inverse piezoelectric effect (see section 3.1.6). It means that we read on the oscilloscope a second harmonic intensity value that was an average on a certain area, so an average on more grains.

The other improvement was about the measure technique. We overcame at once two problems: the lack of homogeneity and to make the measure repeatable. We used the following technique that can be called the *sandwich technique*:

- we put a little amount of powder on an optical window;
- we pressed the powder with another optical window, exactly identical to the other;
- we took off the upper optical window;
- we put the optical window with the powder on the piezoelectric actuator;
- we performed the measure;

- we repeated this procedure for the other samples.

We chose to use two optical windows because they are transparent to both our work wavelength (400nm, 800nm). The best way to perform this measure would require not to take off the upper part of the sandwich, but it wasn't possible. In fact the optical window is $2mm$ thick, while the microscope's working distance is $1.7mm$.

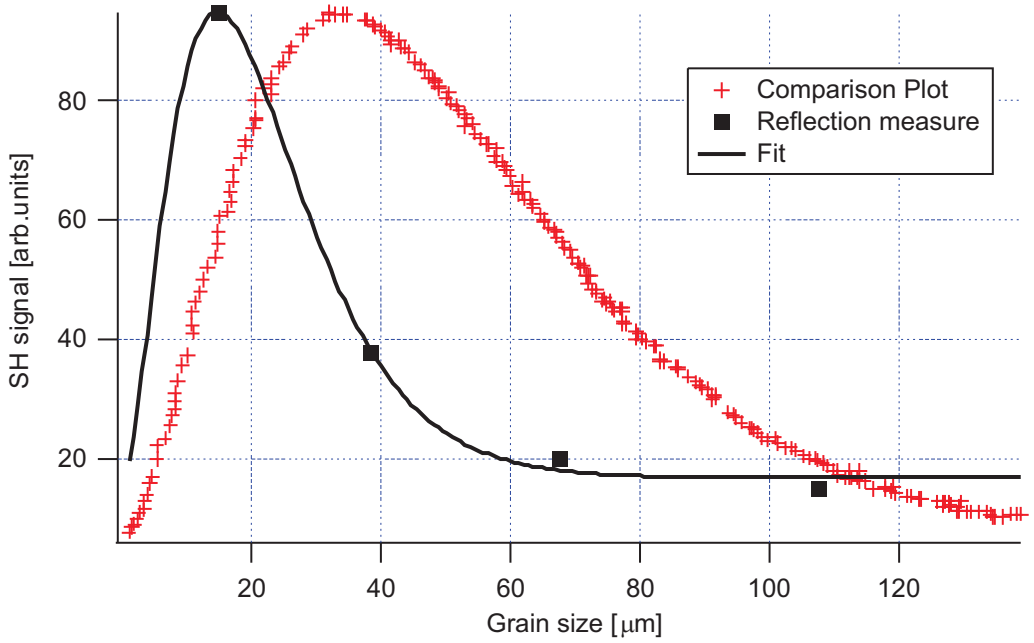

Figure 4.7: Reflection measure

We performed the measure and we handled the data as we had done for the SHG from ceramic glasses measure. So we subtracted the offset before normalizing; then we wanted to put our data on the figure (4.6) plot. So we scaled our data, in order to have our maximum value equal to the maximum value of the plot (4.6).

Figure (4.7) shows our results. We fitted our data with the function

$$f(x) = a + bx^2 e^{-cx}$$

where a,b,c are fit coefficients and x is the grain size. In [2] this is the function of the comparison plot (figure (4.6)).

We don't exactly know the grain size of our samples, we just know the range size of each sample. So we used the mean value of each range to put our data on the plot.

According to figure (4.7) the coherence length of KNS is supposed to be $15\mu m$. This statement has to be confirmed by the transmission measure.

In fact if a different kind of measure gave analogous result, we could conclude that $15\mu m$ is the coherence length of KNS.

4.3.2 Transmission measure

The transmission mode set-up (see section 3.2, figure (3.15)) was used only to perform this measure. The first consideration to do is about the powders: they aren't transparent, they are whitish and opaque. So they transmit just a few light, that's why it was possible to see a transmitted signal only with an extremely thin powder layer on the aspheric lens.

That's the main problem of this measure, it isn't possible to put the same powder layer twice. If the measure was repeated, it could give different data, however the trend should be the same. This was our goal: performing the measure in transmission and finding the same trend we had found by working in reflection.

When the laser beam was focused on the sample, we used all the controllers (translators and tilt) to maximize the second harmonic signal.

We performed the measure twice: the first time we averaged the SH signal on more values measured in different zones of the powder, the second time we measured the maximum value.

We treated the data in both cases as we had done in the previous measure.

The first measure didn't succeed. We think that the cause is the average process: the data are influenced by zones with thicker powder layer, that means less second harmonic intensity. Actually we averaged on a powder layer that was featured by a lack of homogeneity and this is unavoidable. In fact we were forced to put a so little powder amount, otherwise we couldn't have a signal, that it wasn't enough to cover all the lens and to be somehow pressed, in order to have a homogeneous layer.

Hence we decided to perform a measure only on the maximum value of the second harmonic intensity.

Results are reported in figure (4.8), we fitted our data with the same function we used for the reflection measure. The trend is the one expected.

The most interesting thing to do is an overlap of the reflection and transmission measures, that's what we had done in figure (4.9).

It is amazing that the reflection measure and the transmission measure are exactly the same point by point. However the most important results shown in (4.9) are:

- same value of the coherence length
- same trend

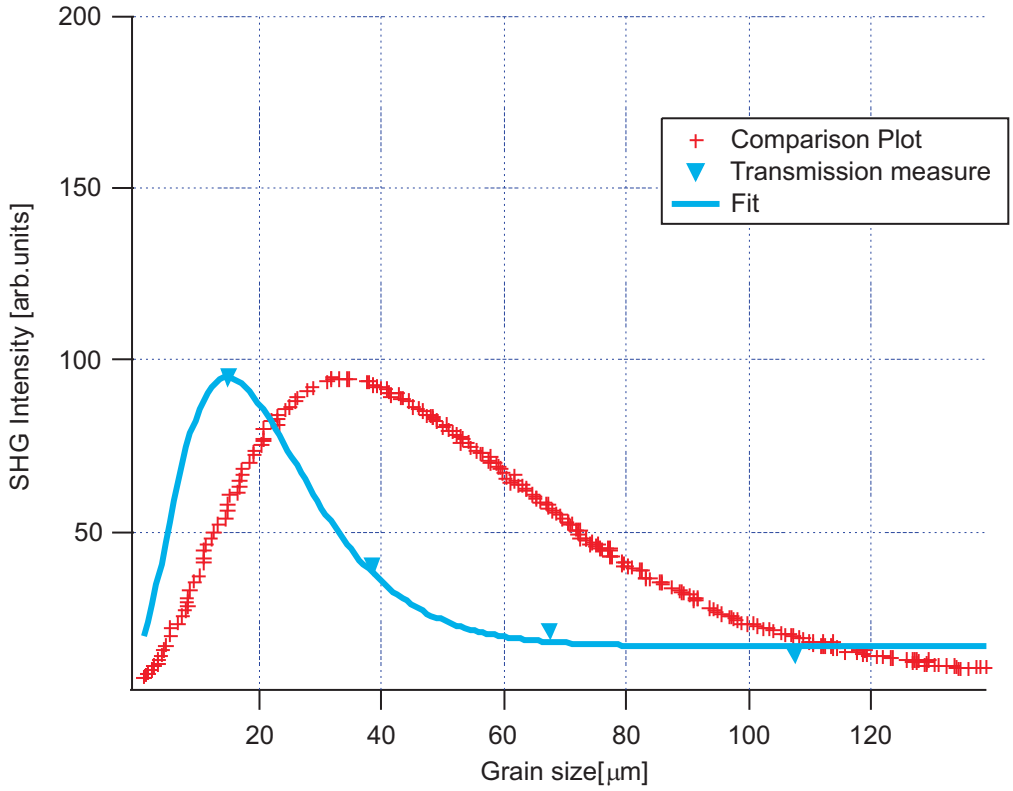

Figure 4.8: Transmission measure

We could so conclude that the coherence length of KNS is $15\mu m$, we have got this result from two totally different measures. Figure (4.9) represents the main goal of this work.

We performed the transmission measure only once, it would be interesting repeat it to control that the trend is actually the same. A further acknowledgement of the SH intensity VS Grain size trend could come from a smaller samples, in fact we hadn't a point in the increasing part of the plot, before the peak.

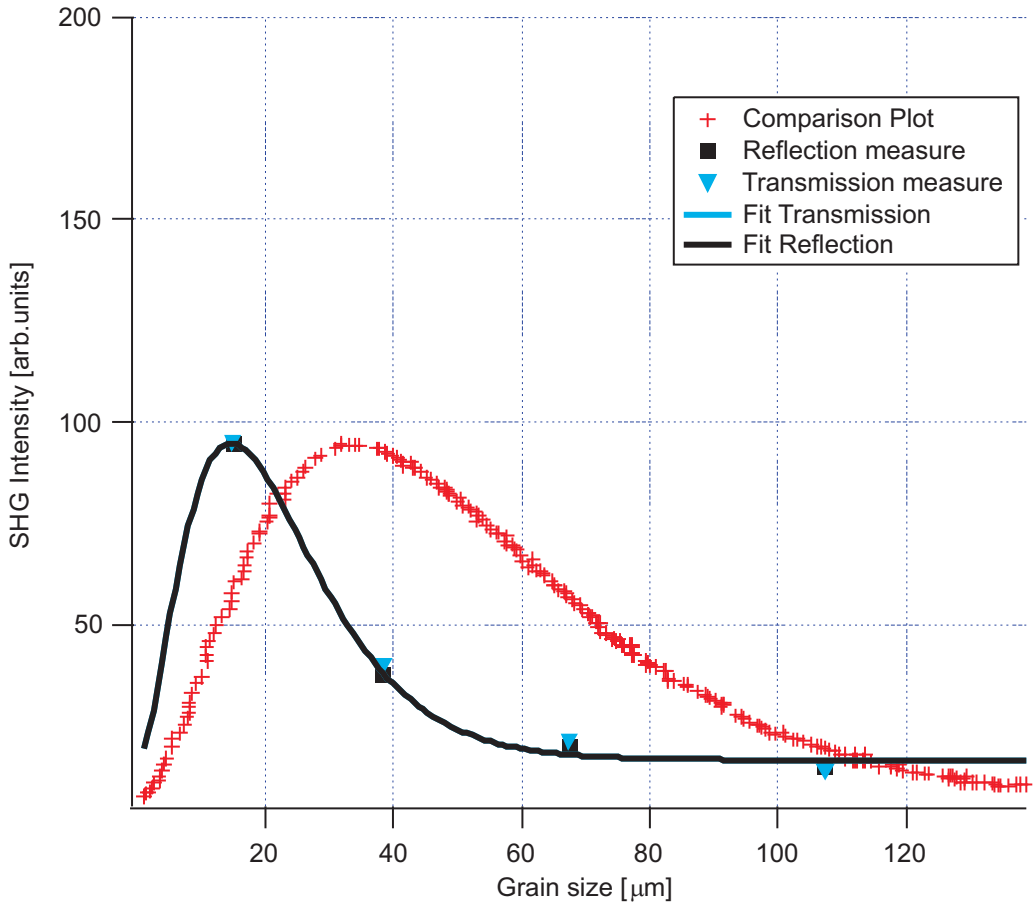

Figure 4.9: Reflection and Transmission measures' comparison

Another interesting and useful measure we didn't perform was the absolute efficiency on KNS powder; we hadn't a reference, like quartz powder for example.

5. Conclusions

We have analyzed the SHG process in four ceramic glasses and we have compared their conversion efficiency with the values measured in [1], because we needed a calibration. The second harmonic signal in all the ceramic glasses is 5 order of magnitude less than a non-phase-matched BBO.

As far as the KNS powders are concerned we have studied the dependency of the second harmonic generation on the grain size. We found a behavior analogous to the one found in literature ([2]).

A powder sample with a smaller grain size value than the ours could give a further confirm, in fact we have no data about the first part of the plot (see figure (4.9)).

We determine the coherence length of the KNS, it is $15\mu m$.

We found the same value with two completely different measure technique: reflection and transmission. We performed the transmission measure only once, so it could be repeated to get a further confirm of our data.

Our result could be used to produce KNS glasses with $15\mu m$ domains, in order to maximize the conversion efficiency.

The evolution of these glasses will be use in integrated chips or optical fibers, in fact they can be formed or processed easily into almost any shape. Besides they don't require a careful alignment of the optical set-up and they are much cheaper than the standard optical converters.

Obviously the development of these disordered systems could bring to appreciable results, only if the conversion efficiency will be improved. In fact we were forced to use the photomultiplier (a device so sensitive that could be used in photon counting experiments) to detect the second harmonic signal produced by the samples.

Bibliography

[1] Luca Bignardi, *Second Harmonic Generation with ultra-short laser pulses in KNS ceramic glasses*

[2] Hart.R,J.W. Swanziger *et al.*, Applied physics letters 6, 85 (2004)

[3] Murugan G.S., Varma K.B.R., Journal of Non-Crystalline Solids 279,1-13 (2001)

[4] Xu X.W., T.C. Chang *et al.*, Journal of Crystal Growth, 225, 458-464 (2001)

[5] Baudrier-Raybaut M., *et al.* Nature 432, 374-376 (2004)

[6] Rosencher E., Vinter B. *Optoelectronics*, Cambridge, 2002

[7] Yariv A., *Quantum electronics*, New York, 1989

[8] Pernice P., Aronne A., *et al.* Journal of Non-Crystalline Solids 306, 238-248 (2002)

[9] Shioya K., Komatsu T., *et al.* Journal of Non-Crystalline Solids 189, 16 (1995)

[10] Sigaev V.N., Pernice P., Aronne A., *et al.* Journal of Non-Crystalline Solids 292, 59 (2001)

[11] Skipetrov Sergey E., Nature 432, 285-286 (2004)

[12] Miller R.C., Phys. Rev. 134, A1313-1319 (1964)

[13] Dewey C.F., Hocker L.O., Appl. Phys. Lett. 26, 442-444 (1975)